Title

New niches for larger phytoplankton in a warmer, more resource-limited ocean

Authors

Suzana G. Leles[1*], Lara Breithaupt[2], Arianna Krinos[3,4], Harriet Alexander[3], Holly V. Moeller[5], Lana Flanjak[6,7], Charlotte Laufkotter[6,7], Elena Litchman[8], María Aranguren-Gassis[9], Naomi M. Levine[1*]

* corresponding authors: leles@usc.edu, n.levine@usc.edu

Affiliations

[1]Department of Marine and Environmental Biology, University of Southern California, CA, USA. [2]Department of Computer Science, Duke University, NC, USA. [3]Biology Department, Woods Hole Oceanographic Institution, Woods Hole, MA, USA. [4]Department of Earth, Environmental, and Planetary Sciences, Brown University, RI, USA. [5]Department of Ecology and Evolutionary Biology, University of California Santa Barbara, CA, USA. [6]Climate and Environmental Physics, Physics Institute, University of Bern, Switzerland. [7]Oeschger Centre for Climate Change Research, University of Bern, Switzerland. [8]W. K. Kellogg Biological Station, Michigan State University, MI, USA [9]Departamento de Ecoloxía e Bioloxía Animal, Grupo de Oceanografía Biolóxica (GOB), Centro de Investigación Mariña (CIM), Universidade de Vigo, 36310 Vigo, Spain

Keywords

climate change, phytoplankton, resource allocation, cell size, proteomic constraints, microbial biogeography

Abstract

Warming and nutrient limitation are major stressors that affect primary production in the ocean, with cascading impacts on the food web. Yet, we lack a mechanistic understanding of how phytoplankton manage the combined stress of heat-damage and nutrient-limitation and the implications of these responses for phytoplankton biogeography. By combining theory, proteome allocation modeling, and climate projections, we identified two potential competing strategies for multi-stressor growth: (1) increase growth temperature optima through higher nutrient uptake efficiency and smaller cells, or (2) invest in heat-mitigation mechanisms achieving higher thermal tolerance at the cost of growth and larger cells. By simulating the optimal metabolic strategies of different phytoplankton functional types across a latitudinal gradient, we found that cyanobacteria are more vulnerable in warmer tropical regions due to greater heat sensitivity and lower storage capacity, indicating a potential ecological niche for larger phytoplankton, such as diatoms, in a warming ocean. Our findings challenge the current understanding that the smallest phytoplankton should prevail across the global ocean as the climate warms.

1 Introduction

Future climate scenarios project an average increase of 1.5°C by 2040 in the global ocean (IPCC, 2023). Ocean warming is expected to promote stronger stratification, potentially decreasing the influx of nutrients from below the mixed layer (Bopp et al., 2001). Changing ocean conditions have already resulted in decreased primary production (Boyce et al., 2010) and shifts in species distributions (Thomas et al., 2012) and size spectra (Atkinson et al., 2024). As phytoplankton drive carbon cycling and fuel the ocean food web (Worden et al., 2015), understanding how these microbes respond to changes in temperature and nutrient availability is critical for predicting ecosystem function as the climate changes (Raven and Geider, 1988; Boyd et al., 2018; Van de Waal and Litchman, 2020).

A key driver of microbial response to resource availability and temperature is cell size, more specifically surface area-to-volume ratio (Litchman et al., 2009; Finkel et al., 2010; Marañón, 2015; Sommer et al., 2017). Under low nutrient concentrations, uptake is limited by molecular diffusion. Thus, a phytoplankter cell can increase nutrient uptake by increasing the number of transporters in the outer membrane (Aksnes and Egge, 1991). As there is a limit to the number of transporters a membrane can support, cells maximize the nutrient flux per unit of cellular volume by decreasing cell size and thereby increasing their surface area-to-volume ratio (Finkel et al., 2010; Sommer et al., 2017; Van de Waal and Litchman, 2020) (Fig. 1). While warming temperatures often result in smaller cell sizes (Atkinson et al., 2003; Daufresne et al., 2009), experimental (Schaum et al., 2018; Liang et al., 2019; Barton et al., 2023; Labban et al., 2023) and field (Hattich et al., 2024) studies have shown that phytoplankton increase their cell volume at critically high temperatures. In a previous study, we suggested that these larger cell sizes are a result of increased investment in energy metabolism and heat-mitigation, both of which require lower surface area-to-volume ratio, i.e., larger cell sizes, to accommodate carbon storage and antioxidant machinery (Leles and Levine, 2023) (Fig. 1). This sets up a challenge for phytoplankton cells facing both nutrient and heat stress: invest in uptake which requires more transporters and higher surface area-to-volume ratios (smaller sizes), or invest in heat-stress mitigation strategies which require lower surface area-to-volume ratios (larger sizes) (Fig. 1).

The global ocean has well known biogeographical distributions of phytoplankton (Longhurst, 2010) with *Prochlorococcus* dominating the oligotrophic gyres and larger eukaryotic phytoplankton thriving in more nutrient-rich temperate and coastal regions (Anderson et al., 2024). Current models predict that, as the climate warms, the oligotrophic gyres will expand poleward resulting in an expanded ecological niche for *Prochlorococcus* (Dutkiewicz et al., 2013; Flombaum et al., 2013). However, these predictions are based on a simplified representation of phytoplankton physi-

ology that does not account for cellular strategies to mitigate heat stress and store carbon, both of which can promote increases in cell volume (Yang et al., 2014; Baroni et al., 2019; Liang et al., 2019; Labban et al., 2023; Marañón et al., 2024; Hattich et al., 2024; Miettinen et al., 2024). In addition, these models assume fixed thermal traits when in reality phytoplankton can shift their thermal optimum for growth (T_{opt}) through evolutionary adaptation and acclimation to changing environmental conditions (Hattich et al., 2024). Empirical studies suggest that the T_{opt} of phytoplankton often shifts left under nutrient limitation resulting in additional growth reductions at high temperatures (Thomas et al., 2017; Bestion et al., 2018). However, some species are able to avoid this "metabolic meltdown" (Huey and Kingsolver, 2019) by increasing their T_{opt} under nutrient stress (Aranguren-Gassis and Litchman, 2020). It remains unclear how physiological responses, such as shifts in T_{opt} and cell size, interact to shape phytoplankton biogeography under climate change.

Here, we investigate underlying mechanisms behind phytoplankton responses to co-occuring heat-stress and nutrient limitation using a cellular allocation model. We demonstrate that T_{opt} can shift to either warmer or cooler temperatures under nitrogen limitation and that this shift is modulated by the heat-mitigation capacity of the cell. We then expand our theoretical predictions by calibrating the model to data for relevant phytoplankton functional types and simulate optimal growth strategies across a latitudinal transect under current and future projections of temperature and nitrate concentrations in the ocean. While the niche of cyanobacteria expands towards higher latitudes, they are more vulnerable in the warmer tropical seas due to their low heat-mitigation capacity and small cell sizes. We thus identify a critical new niche in warm tropical seas where larger phytoplankton, such as *Synechococcus* or even diatoms, might thrive due to their larger flexibility in cell size and thermal tolerance. Our results suggest that representing the interaction between heat-stress and nutrient limitation in climate models is paramount for predicting species extinction and succession.

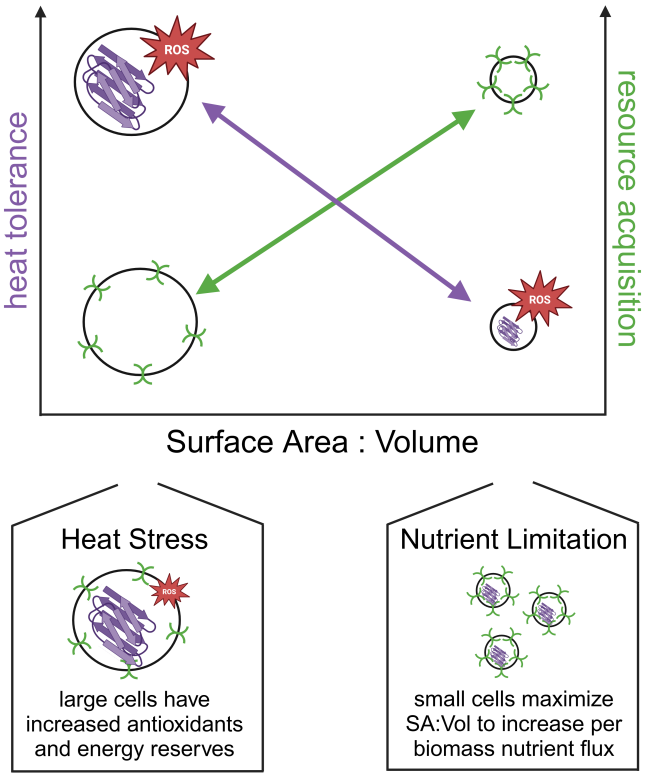

Figure 1: **Predicted trade-off for phytoplankton under multi-stressor growth.** Under nutrient limitation, phytoplankton need to invest more in transporters increasing their surface area-to-volume ratio, which requires smaller cell sizes. Under heat-stress, the cell must invest in heat-mitigation strategies decreasing their surface area-to-volume ratio to accommodate antioxidants and other proteomic investments which requires larger cell sizes. A trade-off between decreasing cell size to optimize nutrient uptake and increasing cell size to optimize heat-mitigation emerges under the multiple stressor scenario.

2 Results

2.1 The proteome allocation model

We used a phytoplankton proteome allocation model to understand the molecular mechanisms behind changes in T_{opt} and cell size under multi-stressor growth (Fig. 1). Here, we expand the model of Leles and Levine (2023) to simulate a range of phytoplankton phenotypes under the multiple stressor condition of heat-stress and resource limitation. We then use the model to simulate phytoplankton growth along a latitudinal gradient under current and future ocean conditions (see Methods).

Our proteome model consists of a system of ordinary differential equations defined as a constrained optimization problem (see Supplemental Methods for complete list of model equations). The model predicts cellular traits and physiological states by maximizing the steady-state growth rate of a phytoplankton cell under specific environmental conditions (i.e., irradiance, external inorganic nitrogen and carbon concentrations, and temperature). Specifically, the model simulates cellular resource allocation by optimizing the relative proteome investment across metabolic functions (e.g., nutrient uptake, biosynthesis, respiration), intracellular macromolecular concentrations (e.g., proteins, carbon storage), and the surface area-to-volume ratio of the phytoplankton cell (Table S1). The model resolves carbon and nitrogen metabolisms, including transport of nitrogen into the cell and synthesis of all critical cellular components. Parameter values are given in the Supplemental Methods (Tables S2 and S3).

Temperature accelerates all enzymatic reactions in the model (Eq. 3, Methods) except photochemical reactions, which we assumed to be temperature independent (Raven and Geider, 1988; Leles and Levine, 2023). Nitrogen transporters have a lower thermal dependency than other reactions in the model based on previous empirical (Kristiansen, 1983; Berges et al., 2002; Baker et al., 2016; Tomczyk et al., 2022) and modeling (Leles and Levine, 2023) studies. All other processes are assumed to have the same thermal dependency (defined by the parameter E_a). Warming also results in protein damage in the model, thus mechanistically representing the decay in growth rates as temperatures increase beyond the optimum. To minimize heat-damage, the model cell can invest in repair pathways and in heat-mitigation strategies, such as producing antioxidant enzymes and/or storing fatty acids (Hemme et al., 2014; Jarc and Petan, 2019; McCain and Bertrand, 2022). Heat-mitigation capacity is controlled by the parameter α, with higher values enabling the cell to build more antioxidant machinery which, in turn, allows the cell to be more efficient at mitigating oxidative stress (Eq. 4, Methods). While high α values provide protection against oxidative stress, this strategy comes with a trade-off of requiring intracellular space and proteomic investment that divests resources away from nutrient acquisition and/or growth.

We solve the proteome model over a range of temperatures and nitrogen concentrations, allowing thermal growth curves to emerge as a function of molecular constraints. Key to our analysis is that we are able to evaluate the underlying physiological and molecular mechanisms driving changes in thermal traits (e.g., T_{opt}) and cell size. The optimal surface area-to-volume ratio of the cell is solved by the model as a function of surface area required for transporters in the cell membrane and cellular volume required for intracellular machinery, such as photosystems, nucleus, and antioxidants. Therefore, our model offers a platform to test, mechanistically, the cell size trade-off that phytoplankton face under the combined effects of heat-stress and nitrogen limitation (Fig. 1).

2.2 Understanding growth trade-offs under multi-stressor conditions

To understand the fundamental trade-offs associated with multi-stressor growth, we simulated phytoplankton cells with varying thermal dependencies (E_a) and heat-damage mitigation ability (α) and analyzed the emergent thermal growth responses (see Sensitivity Analyses, Methods). For this analysis, the cells were otherwise equal (i.e., all other parameters were equal). The model captured the expected trade-offs where warm-adapted cells (higher E_a) have faster growth at higher temperatures but slower growth at lower temperatures (Fig. 2A) and cells with higher heat-mitigation capacity (higher α) survive at higher temperatures at the cost of lower maximum growth rates (Fig. 2B).

The model predicts both increases and decreases in T_{opt} under nitrogen limitation (Figs. 2C and D), consistent with experimental results (Thomas et al., 2017; Bestion et al., 2018; Aranguren-Gassis and Litchman, 2020). The model suggests that warm-adapted cells (higher E_a) are more likely to increase their T_{opt} under nitrogen limitation (Fig. 2D), allowing cells to maximize nitrogen uptake rates at higher temperatures (Fig. 2E). Higher heat-mitigation capacity allows the cell to survive at higher maximum temperatures (Fig. 2F) but it also results in a decrease in T_{opt} and lower maximum growth rates under nutrient stress (Figs. 2D and G). Thus, two competing strategies for coping with multi-stressor conditions emerge from the model results: 'nitrogen-efficient' or 'thermal-tolerant' (Fig. 2C). The 'nitrogen-efficient' strategy couples higher E_a values with lower α values. Higher E_a values allow cells to invest primarily in growth (ribosomes). In turn, lower α values results in less investment in heat-mitigation strategies which allows for smaller cell sizes and more efficient nutrient uptake. This comes with the trade-off that cells are more susceptible to heat-damage and so have lower maximum growth temperatures. Alternatively, the 'thermal-tolerant' strategy cells invest heavily in heat mitigation (higher α). This results in increased proteomic investment in heat mitigation proteins which diverts resources away from growth (ribosomes) and results in lower maximum growth rates (Fig. 2G). This strategy also requires more antioxidant machinery that results in larger cells. However, this investment allows for a higher maximum critical thermal limit (Fig. 2F). Because the 'thermal-tolerant' strategy requires larger cell sizes, cells cannot be both thermally tolerant and nutrient efficient.

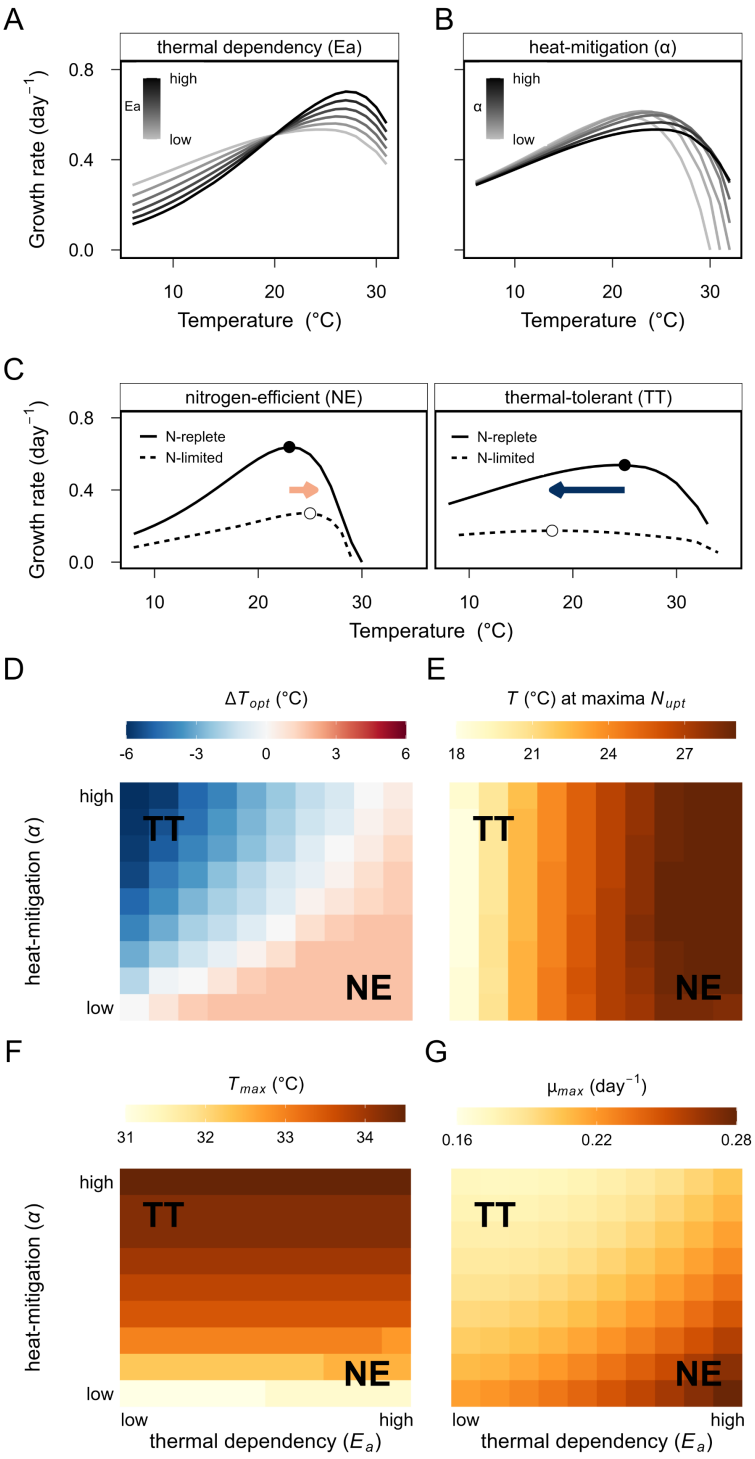

Figure 2: **Growth trade-offs as a function of thermal dependency (Ea) and heat-mitigation capacity (α).** Thermal growth curves under nitrogen-replete conditions are given for (A) cells with variable E_a and (B) cells with variable α. (C) Thermal growth curves indicate shifts in T_{opt} (indicated with an open circle) from N-replete to N-limited conditions as a result of different metabolic strategies. (D) The change in T_{opt} from N-replete to N-limited conditions (Δ T_{opt}). Positive (red) values denote increases in T_{opt} while negative (blue) values indicate decreases in T_{opt}. (E) Temperature (T) where nitrogen uptake rates (N_{upt}) are maximized under N-limited, (F) Maximal growth temperatures (T_{max}) under N-limited, and (G) Maximal growth rates (μ_{max}) under N-limited. The two competing strategies are highlighted: nitrogen-efficient (NE) and thermal-tolerant (TT).

2.3 Predicting phytoplankton optimal growth strategies in a changing ocean

We investigate the implications of different growth strategies in a changing ocean using two contrasting phytoplankton functional types: cyanobacteria and diatoms. Cyanobacteria are small and are optimized for high nutrient use efficiency (Edwards et al., 2012). In contrast, diatoms have larger cell sizes and carry large numbers of genes for mitigating temperature and oxidative stress (Drábková et al., 2007; Bernroitner et al., 2009; Rosenwasser et al., 2014). Here, we parameterized the proteome model to represent these two strategies based on differences in the half-saturation constants for nutrient uptake, thermal traits, and heat-mitigation capacity (Table S3, Methods). To capture the observed global range of diatoms, we simulated both a cold-adapted and a warm-adapted phenotype that differed only in their thermal traits. We validated our model phenotypes against thermal growth data from 167 species obtained from Anderson et al. (2021). The maximum growth rate and slope of the thermal curves for our model phenotypes (Fig. S1) show good agreement with observed values (Fig. 3A). In addition, the emergent cell sizes in the model were consistent with the expected differences between these two groups (Fig. 3B). We also qualitatively validated modeled shifts in proteome investment under heat or nutrient stress using proteomic datasets, based on the up- or down-regulation of specific pathways (Tables S4 and S5, see Methods). Unfortunately, no proteomic datasets were available to validate predictions under combined heat and nutrient stress.

Under heat stress, all phenotypes divested resources away from nitrogen transporters to invest in heat-mitigation strategies and glycolysis to support increased respiration demands (Fig. S3). This trade-off is supported by observed proteomic shifts in the marine diatom *Chaetoceros simplex* (Aranguren-Gassis et al., 2024), where populations down-regulated the investment in nitrogen transporters when grown at temperatures that induced heat-stress, while up-regulating the investment in chaperones, ROS scavenging, heat shock proteins, and glycolysis (Table S4). Under nitrogen stress, all modeled phenotypes maximized the specific affinity for nitrogen uptake by decreasing cell size (Fig. S3). Cells also divested resources away from photosystems, rubisco, ribosomes, and respiration under nitrogen limitation, while investing more in transporters (Fig. S3). These metabolic shifts are overall consistent with empirical observations for both diatoms and cyanobacteria (summarized in Table S5).

Under multi-stressor growth, the 'nitrogen-efficient' strategy allowed cyanobacteria to achieve the fastest maximum growth rates (Fig. S1) and shift their T_{opt} towards warmer temperatures due to their higher nitrogen use efficiency (Figs. 3B and C). However, at critically high temperatures, the 'thermal-tolerant' strategy allowed the warm-adapted diatom to achieve higher carbon and nitrogen use efficiency (Fig. 3C), resulting in better survival at higher maximum temperatures (Fig. S1).

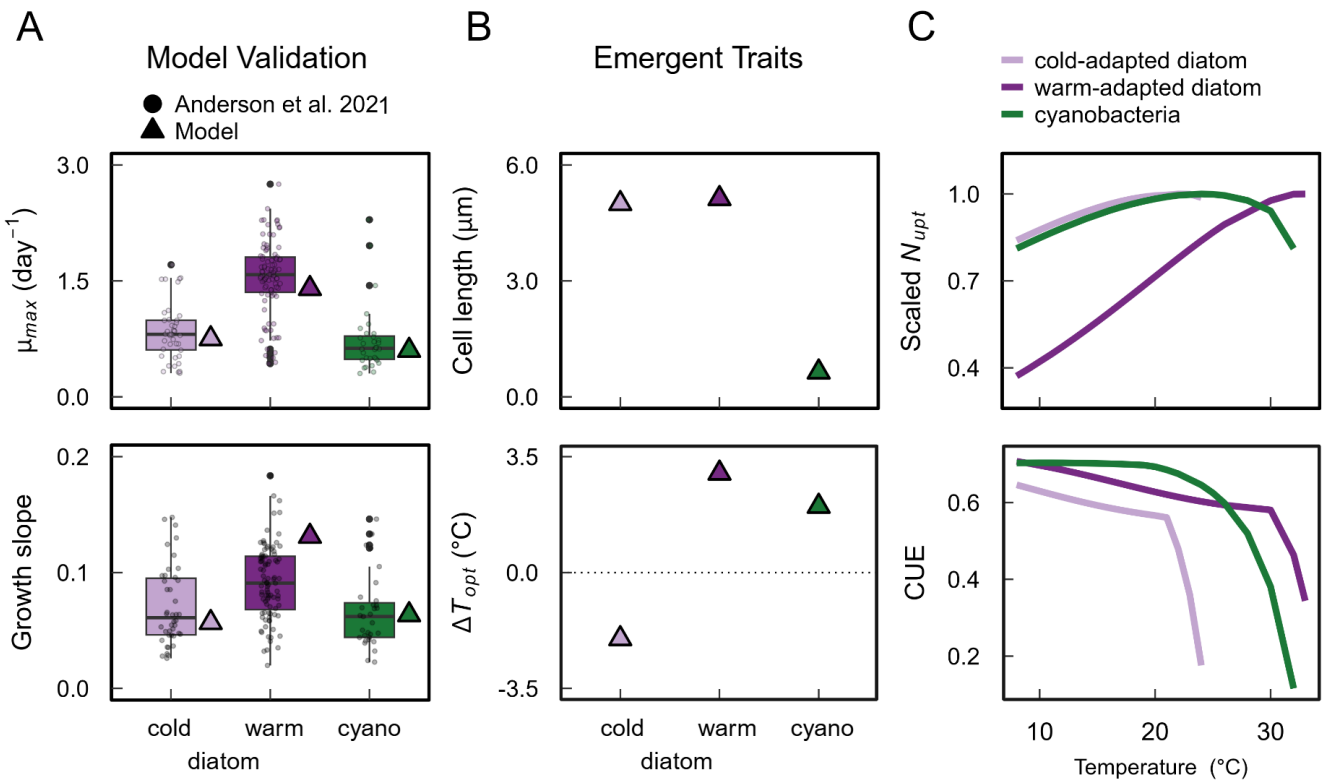

Figure 3: **Emergent traits and trade-offs for different phytoplankton functional types.** (A) Model validation against empirical thermal curve data from Anderson et al. (2021) for cold-adapted (n = 42) and warm-adapted (n = 93) diatoms and cyanobacteria (n = 32) under nitrogen replete conditions. Maximum growth rates (μ_{max}) and the slope at which growth rates increase as a function of temperature are shown. (B) Emergent model cell length at T_{opt} under nitrogen limitation (see Fig. S2 for N-replete conditions) and the shift in T_{opt} from N-limited to N-replete conditions. (C) Model nitrogen uptake rates (N_{upt}) scaled by maximum observed rate and Carbon Use Efficiencies (CUE) under nitrogen limitation. Carbon use efficiency is defined as 1 - respiration/photosynthesis. See Figs. S1 and S3 for full thermal curves and proteome investments in both nutrient regimes.

We use these three phenotypes to investigate optimal growth strategies across a latitudinal transect in the Atlantic Ocean under present day (1980-2000) and future (2080-2100) conditions (see Methods). For this analysis, we use temperature and nitrate concentrations for these two time periods from the CESM-WACCM model (Fig. 4A). The proteome model captured present-day biogeographical conditions. We observed the expected distributions of cold-adapted diatoms at the poles and warm-adapted diatoms in the temperate ocean due to their different thermal dependencies (Figs. 4B and C). The cyanobacteria showed the highest growth potential in the oligotrophic gyres as expected (Fig. S4), especially in the ultra-oligotrophic South Atlantic, due to their high specific nutrient affinity (Figs. 4B and C). The warm-adapted diatom dominated again near the Equator due to increases in nitrate concentrations,

except in the latitudinal range 0-7°N where nitrate concentrations were minimal and temperatures were maximal (Figs. 4B and C).

Under the future climate scenario, temperatures along the transect were on average 2.8 °C warmer (maximum of 4.76 °C) and nitrate concentrations were on average 33% lower (maximum of 86%). The expansion of the oligotrophic gyres, where decreases in nitrate concentrations were greater than the increases in temperature, resulted in the poleward expansion of cyanobacteria due to their higher nutrient affinity, i.e. 'nitrogen-efficient' strategy (Fig. 4C). The cold-adapted diatom phenotype still achieved the highest growth rates in the poles, however, the potential ecological niche for this group was narrower in the future projection due to the higher temperatures (Fig. 4C). The proteome model results also suggest a new niche where the projected increases in temperature will have a larger impact in governing phenotype shift than the projected change in nutrients. This niche occurred in regions of the ocean that are already nutrient-limited under present-day conditions and were predicted to experience significant warming (e.g., 12°S to 22°N). We hypothesize that the 'thermal-tolerant' strategy rather then the 'nutrient-efficient' strategy will have a competitive advantage in these regions, resulting in larger cell sizes and potentially increased abundance of eukaryotic phytoplankton (Figs. 4C and D). While the specific latitudinal range over which these changes would occur depend on the CESM model projections for changes in temperature and nitrate concentrations, our hypothesized shift in ecological niches provide insight into how the phytoplankton community will respond to multi-stressor change.

The underlying metabolic shifts in response to future multi-stressor change varied across oceanographic regions and by phenotype (Figs. 4D and E). At the poles, all phenotypes invested more in transporters (Fig. S5) and decreased their cell size (white filled symbols in Fig. 4D) to maximize nitrogen use efficiency under future more nitrogen limited conditions. This result is consistent with empirical observations that nitrogen limitation plays a more important role than temperature in determining phytoplankton cell size (Sommer et al., 2017). In the tropics, all phenotypes divested away from transporters (Fig. S5) and invested more in photosystems due to critical high temperatures (Fig. 4E), which increased respiration demands and oxidative stress, resulting in lower growth rates relative to current conditions (Fig. S5B). This strategy required larger cell sizes relative to present conditions (black filled symbols in Fig. 4D). While cyanobacteria ('nitrogen-efficient' strategy) increased cell size to accommodate intracellular energy storage compounds to manage increasingly high rates of heat-damage and respiration, the warm-adapted diatom ('thermal-tolerant' strategy) increased cell size to accommodate antioxidants, thus better managing levels of heat-stress. This difference explains why the growth potential of cyanobacteria was lower in the tropics.

Overall, cyanobacteria must devote a larger fraction of the proteome to respiration relative to diatoms due to their lower heat-mitigation capacity (Fig. 4E). As a result, our model suggests that cyanobacteria, in particular the streamlined ultra-oligotrophic 'nitrogen-efficient' *Prochlorococcus*, will have lower metabolic flexibility to manage a warmer climate.

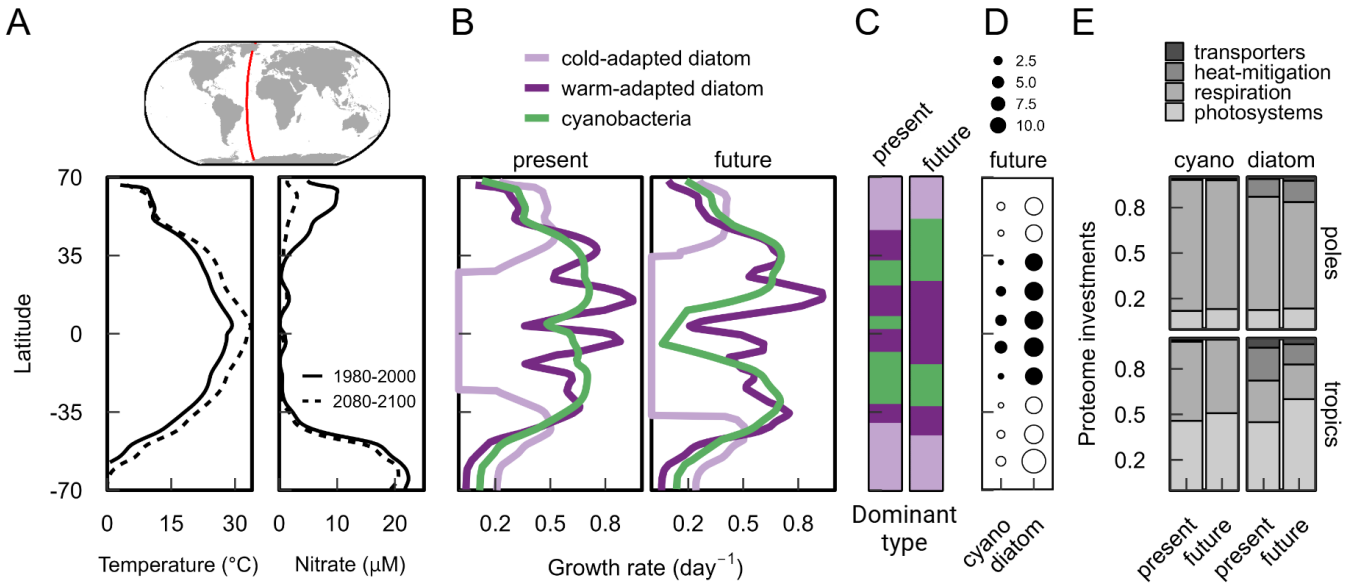

Figure 4: **Phytoplankton optimal growth strategies across a latitudinal gradient in the Atlantic Ocean.** Simulations were run using current (1980-2000) and future (2080-2100) temperature and nitrate concentrations from the CESM-WACCM model (A). Also shown are the optimal growth rates (B), dominant functional type by latitude (C), and optimal cell diameter (μm) under the future climate scenario (D), where white fill and black fill shows decreases and increases in cell size from present to future, respectively. Panel E displays the scaled relative proteome investments (varies between 0 and 1) based on phenotype and climate projection for two distinct regions of the ocean: tropics (8°S-8°N) and poles (50°-70°).

3 Discussion

By combining ecological theory, proteome allocation modeling, and future climate projections, we were able to identify proteomic and cell size constraints underlying phytoplankton response to multi-stressor change. We identified two different strategies that allow phytoplankton to minimize the negative impacts of climate warming under nitrogen limitation: 'nitrogen-efficient' and 'thermal-tolerant'. Cyanobacteria, specifically *Prochlorococcus*, are key examples of the nitrogen-efficient strategy. This strategy has allowed this group to thrive in present day oligotrophic gyres and we predict that their niche will expand polewards under future conditions, consistent with previous studies

(Dutkiewicz et al., 2013; Flombaum et al., 2013). However, we demonstrate that evolving to become maximally nitrogen-efficient, as Prochlorococcus has done, comes at a cost of thermal-tolerance. We therefore predict that future warming will result in a new niche opening in the tropics where 'thermal-tolerant' phytoplankton will gain an advantage over 'nitrogen-efficient' phytoplankton, due to their higher cell size flexibility and ability to manage heat-damage.

Our results highlight that cell size constraints are an important driver of phenotype. All phenotypes were predicted to decrease cell size in the polar and temperate oceans in response to nutrient stress and increase cell size in the tropics due to temperature stress (Fig. 4D). This increase in cell volume for our model diatoms is consistent with previous work which has shown that diatoms and other eukaryotes increase cell size when exposed to temperatures above growth maxima (Liang et al., 2019) and when deprived of nutrients, due to an accumulation of carbohydrates (Baroni et al., 2019; Miettinen et al., 2024) and/or lipids (Yang et al., 2014). Similarly, our model predicted that, in order to survive in the tropics, the cyanobacteria phenotype would need to significantly increase its cell diameter (up to 3-fold) to store carbon and support high respiration costs. This is consistent with recent experiments (Labban et al., 2023) and field manipulative experiments by Marañón et al. (2024), which found that cyanobacteria increased their cell diameter under warming conditions up to 2-fold in the Atlantic Ocean, and that increases in cell volume were associated with slow or negative growth rates.

The closest analogy that we have to future conditions predicted for the tropics is the Red Sea where temperatures can reach record values of 33°C in the surface (Chaidez et al., 2017) and nutrient concentrations can be as low as 0.1 μM (Al-Otaibi et al., 2020). In contrast to the warm oligotrophic gyres in the open ocean, field observations show that the larger cyanobacteria *Synechococcus* can dominate over *Prochlorococcus* in the surface waters of the Red Sea (Al-Otaibi et al., 2020; Coello-Camba and Agustí, 2021). In fact, previous experimental work showed that a Red Sea *Prochlorococcus* strain was unable to survive at temperatures above 30°C (Labban et al., 2023) and field studies show that *Prochlorococcus* is absent in the warmest (> 30°C) waters of the southern Red Sea (Kheireddine et al., 2017). Moreover, the Red Sea has regular nano- and micro- eukaryotes, such as diatoms, and these are found to be dominant in the warm and mesotrophic waters of the southern Red Sea, contributing significantly to primary production (Kheireddine et al., 2017). This is further supported by paleo-oceanographic data showing that diatom-diazotroph associated blooms were wide-spread in warm oligotrophic seas during the Cretaceous when temperatures are estimated to have been approximately 10°C warmer than present day (Kemp and Villareal, 2013). Thus, both our work and experimental and field evidence suggest that elevated temperatures in the equatorial and tropical regions

may favor eukaryotes and larger cyanobacteria relative to *Prochlorococcus*.

We further hypothesize that the greater ability to manage oxidative stress will play a key role in the success of different phenotypes in the future oceans. Diatoms and other eukaryotes have a complex redox system that can sense environmental stressors, like nitrogen limitation (Rosenwasser et al., 2014). Overall, eukaryotes are better at sensing the environment and controlling oxidative stress relative to prokaryotes (Drábková et al., 2007), which is probably related to the lack of a large number of antioxidant genes in the latter (Bernroitner et al., 2009). Previous work suggests that *Prochlorococcus* may have lost many antioxidant genes potentially because they are costly and, instead, rely on other microbes to degrade reactive oxygen species for them (Morris et al., 2012; Weenink et al., 2021). Our model did not account for the potential benefit of these "helpers". Yet, relying on other microbes to perform this important function poses a risk to the adaptive potential of *Prochlorococcus*, as the "helpers" will also rapidly evolve under changing ocean conditions with no guarantee that the current interactions will persist (Hennon et al., 2018; Lu et al., 2024). Finally, diatoms and other eukaryotes have been found to associate symbiotically with nitrogen-fixing cyanobacteria, representing yet another strategy that enables eukaryotes to thrive under nitrogen depleted conditions (Schvarcz et al., 2022; Coale et al., 2024). Exploring how these microbial interactions will shift under multi-stressor changes is an important avenue for future work.

A key limitation of the proteome modeling approach is that it does not account for population dynamics over time, ecological interactions, and thus how phytoplankton shape their environment. However, the trade-offs described here and used to define the 'nitrogen-efficient' and 'thermal-tolerant' strategies can be leveraged to parameterize phytoplankton functional types in biogeochemical models that resolve community dynamics over time (e.g., Dutkiewicz et al. (2021); Anderson et al. (2024)). This is particularly important given that current Earth System Models used by IPCC do not simulate carbon storage nor heat-stress and do not capture the changes in cell size that our model predicts in the tropics. Integrating the insights from cellular scale models into biogeochemical models would allow us to test if these strategies would still be optimal when taking into consideration competition and predation, which are important ecological controls within plankton food webs.

The creation of a new niche for larger phytoplankton in the equatorial and tropical ocean under warming conditions has the potential to reshape microbial interactions, food web structure, and nutrient cycling. Eukaryotic phytoplankton typically release more diverse and abundant organic compounds than cyanobacteria, fueling heterotrophic bacterial growth and enhancing nutrient remineralization (Amin et al., 2012). These interactions can support larger zooplankton previously constrained by the small size of cyanobacterial prey, enhancing trophic transfer efficiency to

higher predators (Ward and Follows, 2016). Moreover, larger phytoplankton have higher cellular carbon content, produce sticky exopolymers that promote particle aggregation (Amin et al., 2012), and are consumed by zooplankton that generate denser fecal pellets. Together, these traits could increase the potential for vertical carbon export to deeper waters, altering the stoichiometry and depth of nutrient recycling.

4 Methods

The model

We use a proteome allocation model modified from Leles and Levine (2023) to predict the optimal metabolic strategy and cell size of a phytoplankton cell under the multi-stressor growth condition of heat and nutrient stress. We further integrate the model to empirical data from 167 species previously compiled by Anderson et al. (2021) to model the optimal strategies of different phytoplankton functional types across a latitudinal transect under current and future ocean conditions. Our coarse-grained model is defined as a constrained optimization problem that maximizes the steady-state growth of the cell. Here, we give the general equations governing the model behavior and focus on the processes relevant for the present work. For the full model equations and list of optimized variables (Table S1) and parameter values (Tables S2 and S3), we refer the reader to the Supplemental Methods and the code available on GitHub (`https://github.com/LevineLab/ProteomePhyto/tree/main`).

The model assumes a cell that is growing exponentially given a certain temperature and nitrogen concentration. The macromolecular concentrations (c) can thus be obtained assuming that the sum of the syntheses rates ($v_{synthesis}$) minus the sum of the degradation rates ($v_{degradation}$) are balanced by the cellular growth rate, μ:

$$\frac{dc}{dt} = \sum v_{synthesis} - \sum v_{degradation} - \mu c \quad = \quad 0. \tag{1}$$

Each reaction rate catalyzed by a given protein i is described following a Michaelis-Menten type equation:

$$v_i = k_i p_i \frac{S_i}{S_i + K_i}, \tag{2}$$

where k_i is the maximum turnover rate per protein, S_i is the substrate concentration, K_i is the half-saturation constant, and p_i is the concentration of protein i. k_i is derived from literature values and corrected to a reference temperature of 20 °C. We assume all reaction rates in the cell increase with temperature following the Arrhenius equation, such that:

$$
\begin{aligned}
k_i &= k_{ref_i} \gamma_{Ta}, \\
\gamma_{Ta} &= \exp\left(\frac{E_a}{R}\left(\frac{1}{T_{ref}} - \frac{1}{T}\right)\right)
\end{aligned}
\tag{3}
$$

where k_{ref_i} is the maximum turnover rate at a reference temperature T_{ref} (in Kelvin) for a given protein i, E_a is the thermal dependency of metabolic rates (eV), R is the Boltzmann's constant (eV K^{-1}) and T is the actual temperature (K). The only exception is the maximum rate of photosynthesis, which we assume to be independent of temperature (Raven and Geider, 1988). All reactions were assumed to have the same E_a, with the exception of nitrogen uptake, for which we halved the thermal dependency relative to other reactions in the model according to previous empirical (Kristiansen, 1983; Berges et al., 2002; Baker et al., 2016) and modeling (Leles and Levine, 2023) studies.

Warming also results in protein damage v_d which increases with increasing temperature, however, cells can invest in heat-mitigation strategies that reduce the impact of heat damage:

$$
\begin{aligned}
v_d &= k_{ref_d} \gamma_{Td} \frac{\alpha}{p_{ox}}, \\
\gamma_{Td} &= \exp\left(\frac{E_d}{R}\left(\frac{1}{T_d} - \frac{1}{T}\right)\right)
\end{aligned}
\tag{4}
$$

in which k_{ref_d} is the maximum rate of damage at a given temperature, E_d is the thermal dependency of protein damage, α is the heat-mitigation capacity of the cell, and p_{ox} is the pool of antioxidant machinery. p_{ox} is constrained to be lower or equal to α. Thus, higher α enables the cell to build more antioxidant machinery p_{ox}, which increases the efficiency of the cell in managing oxidative stress, but it comes at the cost of lower maximum growth rates (Fig. 2B) due to higher intracellular space and proteomic costs required to build p_{ox} that are ultimately divested away from growth. Our model can represent two different strategies in which a cell can mitigate heat-damage: storing lipids

to sequester reactive oxygen species (Jarc and Petan, 2019) or producing antioxidant enzymes to decrease oxidative stress (McCain and Bertrand, 2022). Here, we present the results for the model version in which a cell utilizes lipid storage. The results for antioxidant enzymes are quantitatively the same and are provided in the Supplemental Materials (Fig. S7).

The model optimizes for the surface area-to-volume of the cell. The cell size is a trade-off between 1) surface area required for nitrogen transporters and 2) intracellular space required for intracellular machinery, including photosystems, carbon storage, nucleus, and antioxidants (see Supplementary Methods). The model can be applied to simulate a phytoplankton cell of any shape, but here we assume a spherical cell for simplicity.

Sensitivity analyses

Empirical observations show that phytoplankton species display diverse thermal growth curves (Thomas et al., 2012; Anderson et al., 2021) and sensitivities to oxidative stress (Drábková et al., 2007; Mizrachi et al., 2019). To capture such trait diversity, we varied two parameters in our simulations: the thermal dependency of metabolic reactions (E_a) and the heat-mitigation capacity of the cell (α). We leveraged 167 phytoplankton thermal growth curves from previous compilations (Thomas et al., 2012; Anderson et al., 2021) to select the range of E_a values to test in our sensitivity analyses. Note that the value for E_a in our model corresponds to the metabolic reaction and not necessarily the E_a for growth rates, which is the commonly described parameter in the literature. In turn, the value of α is poorly constrained in the literature. The range of α values used in our simulations was guided by a previous study, which found that phytoplankton sensitivity to oxidative stress can vary up to 10-fold between species (Drábková et al., 2007). We further assumed that, the higher the maximum concentration of antioxidants α, the lower the energetic cost associated with protein damage e_d; all remaining parameter values were held constant for these analyses (Table S2).

We performed simulations for 100 different cells based on a 10x10 grid combining different E_a and α values. We solved the model across a wide range of temperatures for every 0.25 °C to capture the full thermal growth curves and derive the T_{opt} for each phenotype from our simulations. We repeated this process for two different nutrient regimes to simulate nitrogen-replete (DIN = 20 μM) and nitrogen-deplete (DIN = 0.01 μM) conditions. In total, we simulated 200 thermal growth curves and found optimal solutions for approximately 10,000 combinations of temperature, DIN, E_a and α (see Supplementary Methods).

Model comparison against proteomic data

We validated the heat-stress predictions from our model against data from an experimental evolution study that quantified the proteomic responses of the marine diatom *Chaetoceros simplex* (Aranguren-Gassis et al., 2024). In the experiment, protein differential expression was compared between three different populations: ancestral population acclimated to control temperature (25 °C), ancestral population acclimated to heat-stress (31 °C), and warm-evolved population acclimated to heat-stress (34 °C). Functional annotation of all identified proteins and gene ontology (GO) enrichment analysis were conducted using the Omicsbox software (version 1.4.12), employing the Fisher exact test with a false discovery rate (FDR) of 0.05. The analysis utilized the reduced option to provide more specific GO terms (Table S4). We compared our simulations against the proteomic dataset qualitatively, based on the up-regulation or down-regulation of specific pathways. This expands our previous work by providing empirical evidence that supports the modeled trade-off between nutrient acquisition and heat-mitigation for both ancestral and evolved populations. To validate the model predictions between the two different nutrient regimes, we compared model output to literature values for the proteomic responses of different phytoplankton species between nitrogen-replete and nitrogen-deplete conditions (Table S5, Supplementary Methods). No proteomic datasets were available to validate predictions under combined heat and nutrient stress.

Phytoplankton functional types and latitudinal simulations

We solved the proteome model across a latitudinal transect in the Atlantic Ocean, spatially averaging over the longitude range of 330 °to 335 °E, after verifying that temperature and nutrient conditions within this narrow range are relatively uniform. We selected the Atlantic transect for this analysis as it is less dominated by iron limitation compared to the Pacific and therefore offers a more representative environment for examining responses to nitrate limitation. We used historical and future SSP5-8.5 simulations from the CESM2-WACCM model (Danabasoglu et al., 2020) to construct present-day (1980–2000) and future (2080–2100) averages for temperature and nitrate concentrations, both averaged over the upper 20 m of the water column.

We parameterized the model to represent two phytoplankton functional types, cyanobacteria and diatoms, given their importance to global primary production (Dutkiewicz et al., 2021) and their differences in three key parameters: 1) half-saturation constant for nutrient uptake (Edwards et al., 2012), 2) growth thermal dependency (Anderson et al., 2021), and 3) heat-mitigation capacities (Drábková et al., 2007). Given the wide thermal range of diatoms,

we simulated two phenotypes to capture cold- and warm- adapted species. Parameter values were chosen based on previous literature and details are given in the Supplementary Methods (Table S3). To confirm that our parameter choices mimic the general physiology of cyanobacteria, cold-adapted diatoms, and warm-adapted diatoms, we compared the emergent maximum growth rates (μ_{max}) and growth (left) slopes of the thermal curves from our model against data from 167 species previously compiled by Anderson et al. (2021). Diatom species within this dataset with a T_{opt} lower than 20 °C were assigned as cold-adapted. To make this comparison (Figure 3A), we fitted the data to the Norberg equation. We used a log-likelihood function to fit the parameters of the Norberg equation for each experimental dataset from Anderson et al. (2021), then estimated the upper and lower temperature values at which the modeled growth rate was 20 % of its maximum value following Anderson et al. (2021). We calculated the lower and upper slopes of the thermal curve by dividing the difference between the maximum growth rate and 20 % of the maximum growth rate value by the difference between the thermally optimum temperature and the identified temperatures at which growth rate was 20 % of maximum.

We also compared the emergent averaged cell size and nutrient uptake affinities from our model between cyanobacteria and diatoms to make sure these reflected differences observed empirically (Fig. 3B). Finally, we also evaluated if the highest optimal growth rate between cyanobacteria and diatom at any given latitude, as predicted by the proteome model, reflected in higher biomass for that group using simulations from a global model that also considered the different thermal dependencies between these two functional types (Anderson et al., 2024) (Fig. S4).

Acknowledgements and funding sources

We acknowledge funding from the: Simons Foundation through a Simons Postdoctoral Fellowship in Marine Microbial Ecology to SGL (877215), National Science Foundation (NSF) CAREER OCE grant to NML (2044852), Swiss National Science Foundation grant to CL and LF (203448), Xunta de Galicia Postdoctoral Fellowship (2013, 2016) and University of Vigo Research Talent Retention Program (2019) to MAG. AIK was supported by the Simons Collaboration on Computational Biogeochemical Modeling of Marine Ecosystems award (549931).

Author contributions

S.G.L. and N.M.L. conceptualized this study. S.G.L. wrote the initial manuscript, developed the model, and performed data analyses. L.B. developed code to improve the optimization algorithm. A.K. developed code to perform the analyses with the empirically derived thermal growth data. L.F. provided CESM2-WACCM model output. M.A.G. analyzed the proteomic dataset. H.A., H.V.M., C.L., E.L. and other authors revised the initial draft contributing to the final version of this manuscript.

Competing Interests

The authors declare that they have no competing interests.

Data Availability Statement

The model was written in Julia (Bezanson et al., 2017) and the code developed in Leles and Levine (2023) is deposited on Zenodo (DOI: `https://doi.org/10.5281/zenodo.8125732`). The model code used to run the analyses described in the present study are available on GitHub (`https://github.com/LevineLab/ProteomePhyto/tree/main`) and will be added permanently to Zenodo after acceptance. The CESM2-WACCM model output used in this study is available via the Earth System Grid Federation (`https://esgf-node.ipsl.upmc.fr/projects/esgf-ipsl/`).

Code Availability

The model code used to run the analyses described in the present study are available on GitHub (`https://github.com/LevineLab/ProteomePhyto/tree/main`) and will be added permanently to Zenodo after acceptance.

References

Aksnes, D. and Egge, J. (1991). A theoretical model for nutrient uptake in phytoplankton. *Marine ecology progress series. Oldendorf*, 70(1):65–72.

Al-Otaibi, N., Huete-Stauffer, T. M., Calleja, M. L., Irigoien, X., and Morán, X. A. G. (2020). Seasonal variability and vertical distribution of autotrophic and heterotrophic picoplankton in the central red sea. *PeerJ*, 8:e8612.

Amin, S. A., Parker, M. S., and Armbrust, E. V. (2012). Interactions between diatoms and bacteria. *Microbiology and Molecular Biology Reviews*, 76(3):667–684.

Anderson, S., Barton, A., Clayton, S., Dutkiewicz, S., and Rynearson, T. (2021). Marine phytoplankton functional types exhibit diverse responses to thermal change. *Nature communications*, 12(1):6413.

Anderson, S. I., Fronda, C., Barton, A. D., Clayton, S., Rynearson, T. A., and Dutkiewicz, S. (2024). Phytoplankton thermal trait parameterization alters community structure and biogeochemical processes in a modeled ocean. *Global Change Biology*, 30(1):e17093.

Aranguren-Gassis, M., Diz, A. P., Huete-Ortega, M., Allen, A., and Litchman, E. (2024). Evolution of thermal tolerance in marine diatoms: Metabolic strategies under heat stress. *bioRxiv*, pages 2024–11.

Aranguren-Gassis, M., Kremer, C. T., Klausmeier, C. A., and Litchman, E. (2019). Nitrogen limitation inhibits marine diatom adaptation to high temperatures. *Ecology letters*, 22(11):1860–1869.

Aranguren-Gassis, M. and Litchman, E. (2020). Thermal performance of marine diatoms under contrasting nitrate availability. *Journal of Plankton Research*, 42(6):680–688.

Arshad, R., Calvaruso, C., Boekema, E. J., Büchel, C., and Kouřil, R. (2021). Revealing the architecture of the photosynthetic apparatus in the diatom thalassiosira pseudonana. *Plant Physiol.*, 186(4):2124–2136.

Atkinson, A., Rossberg, A. G., Gaedke, U., Sprules, G., Heneghan, R. F., Batziakas, S., Grigoratou, M., Fileman, E., Schmidt, K., and Frangoulis, C. (2024). Steeper size spectra with decreasing phytoplankton biomass indicate strong trophic amplification and future fish declines. *Nature Communications*, 15(1):381.

Atkinson, D., Ciotti, B. J., and Montagnes, D. J. (2003). Protists decrease in size linearly with temperature: ca. 2.5% c- 1. *Proc. Royal Soc. B*, 270(1533):2605–2611.

Baker, K. G., Robinson, C. M., Radford, D. T., McInnes, A. S., Evenhuis, C., and Doblin, M. A. (2016). Thermal performance curves of functional traits aid understanding of thermally induced changes in diatom-mediated biogeochemical fluxes. *Front. Mar. Sci.*, 3:44.

Baroni, É. G., Yap, K. Y., Webley, P. A., Scales, P. J., and Martin, G. J. (2019). The effect of nitrogen depletion on the cell size, shape, density and gravitational settling of nannochloropsis salina, chlorella sp.(marine) and haematococcus pluvialis. *Algal Research*, 39:101454.

Barton, S., Padfield, D., Masterson, A., Buckling, A., Smirnoff, N., and Yvon-Durocher, G. (2023). Comparative experimental evolution reveals species-specific idiosyncrasies in marine phytoplankton adaptation to warming. *Global Change Biology*, 29(18):5261–5275.

Berges, J. A., Varela, D. E., and Harrison, P. J. (2002). Effects of temperature on growth rate, cell composition and nitrogen metabolism in the marine diatom thalassiosira pseudonana (bacillariophyceae). *Mar. Ecol. Prog. Ser.*, 225:139–146.

Bernroitner, M., Zamocky, M., Furtmüller, P. G., Peschek, G. A., and Obinger, C. (2009). Occurrence, phylogeny, structure, and function of catalases and peroxidases in cyanobacteria. *Journal of experimental botany*, 60(2):423–440.

Bestion, E., Schaum, C.-E., and Yvon-Durocher, G. (2018). Nutrient limitation constrains thermal tolerance in freshwater phytoplankton. *Limnology and Oceanography Letters*, 3(6):436–443.

Bezanson, J., Edelman, A., Karpinski, S., and Shah, V. B. (2017). Julia: A fresh approach to numerical computing. *SIAM review*, 59(1):65–98.

Bopp, L., Monfray, P., Aumont, O., Dufresne, J.-L., Le Treut, H., Madec, G., Terray, L., and Orr, J. C. (2001). Potential impact of climate change on marine export production. *Global Biogeochemical Cycles*, 15(1):81–99.

Boyce, D. G., Lewis, M. R., and Worm, B. (2010). Global phytoplankton decline over the past century. *Nature*, 466(7306):591–596.

Boyd, P. W., Collins, S., Dupont, S., Fabricius, K., Gattuso, J.-P., Havenhand, J., Hutchins, D. A., Riebesell, U., Rintoul, M. S., Vichi, M., et al. (2018). Experimental strategies to assess the biological ramifications of multiple drivers of global ocean change—a review. *Global change biology*, 24(6):2239–2261.

Chaidez, V., Dreano, D., Agusti, S., Duarte, C., and Hoteit, I. (2017). Decadal trends in red sea maximum surface temperature, sci. rep., 7, 8144.

Chen, X.-H., Li, Y.-Y., Zhang, H., Liu, J.-L., Xie, Z.-X., Lin, L., and Wang, D.-Z. (2018). Quantitative proteomics reveals common and specific responses of a marine diatom thalassiosira pseudonana to different macronutrient deficiencies. *Frontiers in Microbiology*, 9:2761.

Coale, T. H., Loconte, V., Turk-Kubo, K. A., Vanslembrouck, B., Mak, W. K. E., Cheung, S., Ekman, A., Chen, J.-H., Hagino, K., Takano, Y., et al. (2024). Nitrogen-fixing organelle in a marine alga. *Science*, 384(6692):217–222.

Coello-Camba, A. and Agustí, S. (2021). Picophytoplankton niche partitioning in the warmest oligotrophic sea. *Frontiers in Marine Science*, 8:651877.

Danabasoglu, G., Lamarque, J.-F., Bacmeister, J., Bailey, D., DuVivier, A., Edwards, J., Emmons, L., Fasullo, J., Garcia, R., Gettelman, A., et al. (2020). The community earth system model version 2 (cesm2). *Journal of Advances in Modeling Earth Systems*, 12(2):e2019MS001916.

Daufresne, M., Lengfellner, K., and Sommer, U. (2009). Global warming benefits the small in aquatic ecosystems. *Proc. Natl. Acad. Sci.*, 106(31):12788–12793.

Domínguez-Martín, M. A., Gómez-Baena, G., Díez, J., López-Grueso, M. J., Beynon, R. J., and García-Fernández, J. M. (2017). Quantitative proteomics shows extensive remodeling induced by nitrogen limitation in prochlorococcus marinus ss120. *MSystems*, 2(3):10–1128.

Drábková, M., Admiraal, W., and Maršálek, B. (2007). Combined exposure to hydrogen peroxide and light selective effects on cyanobacteria, green algae, and diatoms. *Environmental science & technology*, 41(1):309–314.

Dutkiewicz, S., Boyd, P. W., and Riebesell, U. (2021). Exploring biogeochemical and ecological redundancy in phytoplankton communities in the global ocean. *Global change biology*, 27(6):1196–1213.

Dutkiewicz, S., Scott, J. R., and Follows, M. (2013). Winners and losers: Ecological and biogeochemical changes in a warming ocean. *Global Biogeochemical Cycles*, 27(2):463–477.

Edwards, K. F., Thomas, M. K., Klausmeier, C. A., and Litchman, E. (2012). Allometric scaling and taxonomic variation in nutrient utilization traits and maximum growth rate of phytoplankton. *Limnology and Oceanography*, 57(2):554–566.

Finkel, Z. V., Beardall, J., Flynn, K. J., Quigg, A., Rees, T. A. V., and Raven, J. A. (2010). Phytoplankton in a changing world: cell size and elemental stoichiometry. *Journal of plankton research*, 32(1):119–137.

Finkel, Z. V., Follows, M. J., Liefer, J. D., Brown, C. M., Benner, I., and Irwin, A. J. (2016). Phylogenetic diversity in the macromolecular composition of microalgae. *PLoS One*, 11(5):e0155977.

Flombaum, P., Gallegos, J. L., Gordillo, R. A., Rincón, J., Zabala, L. L., Jiao, N., Karl, D. M., Li, W. K., Lomas, M. W., Veneziano, D., et al. (2013). Present and future global distributions of the marine cyanobacteria prochlorococcus and synechococcus. *Proceedings of the National Academy of Sciences*, 110(24):9824–9829.

Hattich, G., Jokinen, S., Sildever, S., Gareis, M., Heikkinen, J., Junghardt, N., Segovia, M., Machado, M., and Sjöqvist, C. (2024). Temperature optima of a natural diatom population increases as global warming proceeds. *Nature Climate Change*, 14(5):518–525.

Hemme, D., Veyel, D., Mühlhaus, T., Sommer, F., Jüppner, J., Unger, A.-K., Sandmann, M., Fehrle, I., Schönfelder, S., Steup, M., et al. (2014). Systems-wide analysis of acclimation responses to long-term heat stress and recovery in the photosynthetic model organism chlamydomonas reinhardtii. *Plant Cell*, 26(11):4270–4297.

Hennon, G. M., Morris, J. J., Haley, S. T., Zinser, E. R., Durrant, A. R., Entwistle, E., Dokland, T., and Dyhrman, S. T. (2018). The impact of elevated co2 on prochlorococcus and microbial interactions with 'helper'bacterium alteromonas. *The ISME journal*, 12(2):520–531.

Huey, R. B. and Kingsolver, J. G. (2019). Climate warming, resource availability, and the metabolic meltdown of ectotherms. *The American Naturalist*, 194(6):E140–E150.

IPCC (2023). Climate change 2023: Synthesis report. contribution of working groups i, ii and iii to the sixth assessment report of the intergovernmental panel on climate change. `https://www.ipcc.ch/report/ar6/syr/`. Core Writing Team, H. Lee and J. Romero (eds.).

Jarc, E. and Petan, T. (2019). Focus: Organelles: Lipid droplets and the management of cellular stress. *Yale J. Biol. Med.*, 92(3):435.

Kemp, A. E. and Villareal, T. A. (2013). High diatom production and export in stratified waters–a potential negative feedback to global warming. *Progress in Oceanography*, 119:4–23.

Kheireddine, M., Ouhssain, M., Claustre, H., Uitz, J., Gentili, B., and Jones, B. H. (2017). Assessing pigment-based phytoplankton community distributions in the red sea. *Frontiers in Marine Science*, 4:132.

Kristiansen, S. (1983). The temperature optimum of the nitrate reductase assay for marine phytoplankton 1. *Limnol. Oceanogr.*, 28(4):776–780.

Labban, A., Shibl, A. A., Calleja, M. L., Hong, P.-Y., and Morán, X. A. G. (2023). Growth dynamics and transcriptional responses of a red sea prochlorococcus strain to varying temperatures. *Environmental microbiology*, 25(5):1007–1021.

Leles, S. G. and Levine, N. M. (2023). Mechanistic constraints on the trade-off between photosynthesis and respiration in response to warming. *Science Advances*, 9(35):eadh8043.

Liang, Y., Koester, J. A., Liefer, J. D., Irwin, A. J., and Finkel, Z. V. (2019). Molecular mechanisms of temperature acclimation and adaptation in marine diatoms. *The ISME Journal*, 13(10):2415–2425.

Litchman, E., Klausmeier, C., and Yoshiyama, K. (2009). Contrasting size evolution in marine and freshwater diatoms. *Proceedings of the National Academy of Sciences*, 106(8):2665–2670.

Longhurst, A. R. (2010). *Ecological geography of the sea*. Elsevier.

Lu, Z., Entwistle, E., Kuhl, M. D., Durrant, A. R., Filho, M. M. B., Goswami, A., and Morris, J. (2024). Marine phytoplankton and heterotrophic bacteria rapidly adapt to future pco2 conditions in experimental co-cultures. *bioRxiv*, pages 2024–02.

Malerba, M. E. and Marshall, D. J. (2021). Larger cells have relatively smaller nuclei across the tree of life. *Evolution Letters*, 5(4):306–314.

Marañón, E. (2015). Cell size as a key determinant of phytoplankton metabolism and community structure. *Annual review of marine science*, 7(1):241–264.

Marañón, E., Fernández-González, C., and Tarran, G. A. (2024). Effect of temperature, nutrients and growth rate on picophytoplankton cell size across the atlantic ocean. *Scientific Reports*, 14(1):28034.

McCain, J. S. P. and Bertrand, E. M. (2022). Phytoplankton antioxidant systems and their contributions to cellular elemental stoichiometry. *Limnology and Oceanography Letters*, 7(2):96–111.

Miettinen, T. P., Gomez, A. L., Wu, Y., Wu, W., Usherwood, T. R., Hwang, Y., Roller, B. R., Polz, M. F., and Manalis, S. R. (2024). Cell size, density, and nutrient dependency of unicellular algal gravitational sinking velocities. *Science Advances*, 10(27):eadn8356.

Mizrachi, A., Graff van Creveld, S., Shapiro, O. H., Rosenwasser, S., and Vardi, A. (2019). Light-dependent single-cell heterogeneity in the chloroplast redox state regulates cell fate in a marine diatom. *Elife*, 8:e47732.

Morris, J. J., Lenski, R. E., and Zinser, E. R. (2012). The black queen hypothesis: evolution of dependencies through adaptive gene loss. *MBio*, 3(2):10–1128.

Raven, J. A. and Geider, R. J. (1988). Temperature and algal growth. *New Phytol.*, 110(4):441–461.

Remmers, I. M., D'Adamo, S., Martens, D. E., de Vos, R. C., Mumm, R., America, A. H., Cordewener, J. H., Bakker, L. V., Peters, S. A., Wijffels, R. H., et al. (2018). Orchestration of transcriptome, proteome and metabolome in the diatom phaeodactylum tricornutum during nitrogen limitation. *Algal research*, 35:33–49.

Rosenwasser, S., Graff van Creveld, S., Schatz, D., Malitsky, S., Tzfadia, O., Aharoni, A., Levin, Y., Gabashvili, A., Feldmesser, E., and Vardi, A. (2014). Mapping the diatom redox-sensitive proteome provides insight into response to nitrogen stress in the marine environment. *Proceedings of the National Academy of Sciences*, 111(7):2740–2745.

Schaum, C.-E., Buckling, A., Smirnoff, N., Studholme, D., and Yvon-Durocher, G. (2018). Environmental fluctuations accelerate molecular evolution of thermal tolerance in a marine diatom. *Nature communications*, 9(1):1719.

Schvarcz, C. R., Wilson, S. T., Caffin, M., Stancheva, R., Li, Q., Turk-Kubo, K. A., White, A. E., Karl, D. M., Zehr, J. P., and Steward, G. F. (2022). Overlooked and widespread pennate diatom-diazotroph symbioses in the sea. *Nature communications*, 13(1):799.

Sommer, U., Peter, K. H., Genitsaris, S., and Moustaka-Gouni, M. (2017). Do marine phytoplankton follow b ergmann's rule sensu lato? *Biological Reviews*, 92(2):1011–1026.

Thomas, M. K., Aranguren-Gassis, M., Kremer, C. T., Gould, M. R., Anderson, K., Klausmeier, C. A., and Litchman, E. (2017). Temperature–nutrient interactions exacerbate sensitivity to warming in phytoplankton. *Global change biology*, 23(8):3269–3280.

Thomas, M. K., Kremer, C. T., Klausmeier, C. A., and Litchman, E. (2012). A global pattern of thermal adaptation in marine phytoplankton. *Science*, 338(6110):1085–1088.

Tomczyk, N., Rosemond, A., Kaz, A., and Benstead, J. (2022). Contrasting activation energies of respiration and nutrient uptake drive lower ecosystem-level uptake at higher temperatures. *Biogeosci.*, pages 1–21.

Van de Waal, D. B. and Litchman, E. (2020). Multiple global change stressor effects on phytoplankton nutrient acquisition in a future ocean. *Philosophical Transactions of the Royal Society B*, 375(1798):20190706.

Ward, B. A. and Follows, M. J. (2016). Marine mixotrophy increases trophic transfer efficiency, mean organism size, and vertical carbon flux. *Proceedings of the National Academy of Sciences*, 113(11):2958–2963.

Weenink, E. F., Matthijs, H. C., Schuurmans, J. M., Piel, T., van Herk, M. J., Sigon, C. A., Visser, P. M., and Huisman, J. (2021). Interspecific protection against oxidative stress: green algae protect harmful cyanobacteria against hydrogen peroxide. *Environmental Microbiology*, 23(5):2404–2419.

Worden, A. Z., Follows, M. J., Giovannoni, S. J., Wilken, S., Zimmerman, A. E., and Keeling, P. J. (2015). Rethinking the marine carbon cycle: factoring in the multifarious lifestyles of microbes. *Science*, 347(6223):1257594.

Yang, Z.-K., Ma, Y.-H., Zheng, J.-W., Yang, W.-D., Liu, J.-S., and Li, H.-Y. (2014). Proteomics to reveal metabolic network shifts towards lipid accumulation following nitrogen deprivation in the diatom phaeodactylum tricornutum. *Journal of applied phycology*, 26:73–82.

Supplementary Materials for

New niches for larger phytoplankton in a warmer, more resource-limited ocean

Suzana G. Leles[1*], Lara Breithaupt[2], Arianna Krinos[3], Harriet Alexander[3], Holly V. Moeller[4], Lana Flanjak[5,6], Charlotte Laufkotter[5,6], Elena Litchman[7], Marìa Aranguren-Gassis[8], Naomi M. Levine[1*]

Corresponding authors: leles@usc.edu, n.levine@usc.edu

This PDF file includes:

- Supplementary Methods
- Supplemental Figures
- Supplemental Tables

Supplementary Methods

Model equations

The model is fully defined below. A list of the optimized variables is given in Table S1. Detailed description for each of the metabolic pathways are described in Leles and Levine (2023) except for additions/modifications to the model which are then described here. Descriptions of the constant parameters are given in the following section as well as Tables S2 and S3.

C1-C8: Steady-state growth of proteins

$$\frac{d(p_p + p_{dp})}{dt} = \phi_p v_{ri} \frac{1}{\eta_p} - \mu(p_p + p_{dp}) = 0$$
$$\frac{dp_{ru}}{dt} = \phi_{ru} v_{ri} \frac{1}{\eta_{ru}} - \mu p_{ru} = 0$$
$$\frac{dp_{tr}}{dt} = \phi_{tr} v_{ri} \frac{1}{\eta_{tr}} - \mu p_{tr} = 0$$
$$\frac{dp_{ri}}{dt} = \phi_{ri} v_{ri} \frac{1}{\eta_{ri}} - \mu p_{ri} = 0$$
$$\frac{dp_{gl}}{dt} = \phi_{gl} v_{ri} \frac{1}{\eta_{gl}} - \mu p_{gl} = 0$$
$$\frac{dp_{lb}}{dt} = \phi_{lb} v_{ri} \frac{1}{\eta_{lb}} - \mu p_{lb} = 0$$
$$\frac{dp_{ld}}{dt} = \phi_{ld} v_{ri} \frac{1}{\eta_{ld}} - \mu p_{ld} = 0$$
$$\frac{dp_{re}}{dt} = \phi_{re} v_{ri} \frac{1}{\eta_{re}} - \mu p_{re} = 0$$

C9-C12: Steady-state growth of other macromolecules

$$\frac{dc_{ic}}{dt} = v_{ru} - v_{ri}\eta_{aac} - v_{lb} - v_{gl} - \mu c_{ic} = 0$$
$$\frac{dc_{in}}{dt} = v_{tr} - v_{ri}\eta_{aan} - \mu c_{in} = 0$$
$$\frac{dc_{lm}}{dt} = \alpha_{lm} v_{lb} \frac{1}{\eta_{lic}} - \mu c_{lm} = 0$$
$$\frac{dp_{ox}}{dt} = \alpha_{tag} v_{lb} \frac{1}{\eta_{lic}} - \mu p_{ox} = 0$$

C13: Proteome investments, in which i represents protein pools

$$\sum \phi_i = 0.5$$

C14: Fractions of the lipid synthesis flux:

$$\alpha_{lm} + \alpha_{tag} + \alpha_{ld} = 1.0$$

C15: Fraction of damaged photosystems (a function of heat damage and repair)

$$\frac{p_{dp}}{p_{dp} + p_p} = \frac{k_d p_p \frac{\alpha}{p_{ox}}}{k_{re} p_{re}}$$

C16: Constraint on the maximum concentration of stored lipids that mitigate damage

$$p_{ox} \leq \alpha_{min} + \alpha$$

C18: Membrane integrity

$$\frac{p_{tr}}{c_{lm}} \leq M_{min} + M_{max} \gamma_{Tm}$$

C19: Lipid degradation:

$$v_{ld} = \alpha_{lb} v_{lb}$$

C20-22: Energy metabolism

$$e_p v_p \geq e_{ru} v_{ru}$$

$$e_{cost} \leq (e_p v_p - e_{ru} v_{ru})$$

where, $e_{cost} = e_{tr}v_{tr} + e_{ri}v_{ri} + e_{lb}v_{lb} + e_d v_d + e_f v_{re}$

$$f_{dr}e_{cost} \leq e_{gl}v_{gl} + e_{ld}v_{ld}$$

C23: Space constraint

$$1 = (p_{tr}s_{tr} + c_{lm}s_{lm})\beta$$

C24: Density constraint, in which k indicates all pools of the cell except for photosystems, lipid storage and membrane components

$$\sum c_k \frac{1}{\eta_k} \leq D_{max}\frac{V}{V_{tot}}$$

where, $\frac{V}{V_{tot}} = 1 - (p_p + p_{dp})V_p - (c_{li} + c_{tag})V_{li} - \frac{V_{nu}}{V_{tot}}$

Reaction rates are defined as following:

$$v_p = k_{ref_p} p_p \frac{I}{I + K_p}$$
$$v_{ru} = k_{ref_{ru}} \gamma_{Ta} p_{ru} \frac{DIC}{DIC + K_{ru}}$$
$$v_{tr} = k_{ref_{tr}} \gamma_{Ta} p_{tr} \frac{DIN}{DIN + K_{tr}}$$
$$v_{ri} = k_{ref_{ri}} \gamma_{Ta} p_{ri} \frac{c_{ic}}{c_{ic} + K_{ic}} \frac{c_{in}}{c_{in} + K_{in}}$$
$$v_{gl} = k_{ref_{gl}} \gamma_{Ta} p_{gl}$$
$$v_{lb} = k_{ref_{lb}} \gamma_{Ta} p_{lb} \frac{c_{ic}}{c_{ic} + K_{lb}}$$
$$v_{ld} = k_{ref_{ld}} \gamma_{Ta} p_{ld}$$
$$v_d = k_{ref_d} \gamma_{Td} p_p \frac{\alpha}{p_{ox}}$$
$$v_{re} = k_{ref_{re}} \gamma_{Ta} p_{re} \frac{p_{dp}}{p_{dp} + p_p}$$

Temperature effects:

$$\gamma_{Ta} = exp(\frac{E_a}{R}(\frac{1}{T_{ref}} - \frac{1}{T}))$$
$$\gamma_{Td} = exp(\frac{E_d}{R}(\frac{1}{T_d} - \frac{1}{T}))$$
$$\gamma_{Tm} = (\frac{T_{max} - T}{T_{max} - T_{min}})$$

Number of molecules of nitrogen per amino acid:

$$\eta_{aan} = \eta_{aac} \sum \phi_i q_i$$

Estimated storage pools that fuel dark respiration:

$$c_{gu} = v_{gl}\frac{1}{\eta_{guc}}td$$
$$c_{li} = v_{ld}\frac{1}{\eta_{lic}}td$$

Cell nitrogen to carbon quota (q_{cell}), in which i represents protein pools and η_i represents the molecular weight of proteins in units of aa protein^{-1}:

$$q_{cell} = \frac{\sum c_i\eta_i\eta_{aac}q_i + c_{in}}{\sum c_i\eta_i\eta_{aac} + c_{ic} + (c_{lm} + c_{li} + c_{tag})\eta_{lic} + c_{gu}\eta_{guc}}$$

Constraining the minimal model cell size

The proteome allocation model solves for the optimal concentration of different macromolecules in the cell given a specific set of environmental conditions. We impose a constraint on the maximum intracellular density of macromolecules (D_{max}) such that, if the optimal metabolic strategy involves building more proteins and the cell is at D_{max}, the cell must increase its cell size. The volume of the cell is defined by the volume occupied by photosystems and stored lipids as well as all other macromolecules, following Eqs. 41-43 in Leles and Levine (2023). These constraints effectively keep cell size from increasing indefinitely in our model. In order to constraint the minimal size of our modeled cell, we require the model to account for the intracellular space taken up by the cellular nucleus (V_{nu}). Thus we modify Eq. 41 from Leles and Levine (2023):

$$V_{tot} = V + (n_p + n_{dp})V_p + (n_{li} + n_{tag})V_{li} + V_{nu}, \tag{5}$$

in which V_{tot} is the total cellular volume, V is the volume occupied by all macromolecules with the exception of photosystems, stored lipids, and nucleus. n_p and n_{dp} are the total number of functional and damaged photosystems, respectively, and n_{li} and n_{tag} are the total number of stored lipids required to regulate oxidative stress and to fuel

respiration, respectively. V_p and V_{li} correspond to the volume of photosystem and stored lipid molecules, respectively.

Parameter values

The parameters used to define the different phytoplankton functional types can be found in Table S3. Below we describe in detail our choices for each of these parameters. All other parameter values of the model were kept the same and can be found in Table S2; for detailed description on the choice of these parameter values and respective references please refer to the supplemental methods in Leles and Levine (2023).

E_a: this parameter sets the slope at which metabolic rates in the model increase exponentially as a function of temperature. To parameterize E_a, we derived the growth (left) slope of the thermal growth curves for the different functional types from empirical data available for 167 species of phytoplankton based on the compilation in Anderson et al. (2021) and validated our model against the averaged values obtained from empirical observations (Fig. 3A).

T_d: similarly, the heat-stress temperature was defined based on averaged values from the same dataset compiled in Anderson et al. (2021).

K_{tr}: the half-saturation for nitrogen uptake was derived from Figure 1B in Edwards et al. (2012).

V_p: the average volume occupied by a photosystem molecule is $3 \times 10^{-5} \mu m^3$ for *Thalassiosira pseudonana* (Arshad et al., 2021) and between 1×10^{-6} - 2×10^{-5} μm^3 for the cyanobacteria *Synechococcus* (BioNumbers: ID103908 and ID103909).

V_{nu}: the nucleus volume was derived from Malerba and Marshall (2021), in which the nucleus volume was given for several species of phytoplankton.

α: the maximum concentration of antioxidants (i.e. stored lipids) in the cell (not used to fuel dark respiration) was constrained based on the average fraction of the cellular volume that is occupied by lipids, i.e. 20% Finkel et al. (2016), resulting in a maximum value of 2×10^7 molecules μm^{-3}.

e_d: we assumed that the rate of heat-damage scales with $c_{tag_{max}}$ so that the cost is higher for cyanobacteria based on their higher sensitivity to heat stress (Drábková et al., 2007), as following: $e_d = \frac{2\times10^7}{c_{tag_{max}}}$.

Improving optimization algorithm

The proteome model solves for the optimal steady-state solution which maximizes growth rates. However, sometimes the optimizer can get stuck in a local minimum instead of finding the global minimum. This can occur for many reasons including the optimizer 'timing out' due to the optimization surface being too flat or a poor initial conditions. As this work required solving for 10,000 combinations of trait values (model parameters) and environmental conditions, we needed to develop a pipeline for ensuring that the optimizer indeed found the global minimum. We used an iterative approach based on the assumption that the model solutions would be either continuous or exhibit a relatively small number of states across the tested environmental conditions.

We first conducted a set of simulations across the environmental gradient (e.g., temperature) using several random initial guesses. We used the optimized solutions from these initial runs to identify 'anomalous' solutions that might be local minima. Specifically, we used a moving average approach relying on tangent line calculations to evaluate the rate of change between consecutive solutions across a temperature gradient. An abrupt change in the tangent between consecutive data points resulted in the solution being flagged as potentially 'anomalous'. Solutions which violated biologically realistic bounds for key variables were also flagged. We used the following bounds for each of the key variables: growth rates (0.001-5 day^-1), cell length (0.001-300 μm), and nitrogen to carbon quota of the cell (0.005-0.5 mol N:mol C). We then identified, for each 'anomalous' solution, the closest preceding and succeeding 'good' solution (i.e., solutions not flagged as anomalous). The initial conditions (starting guesses) for the optimizer were then derived by extrapolating between these closest good solutions using a linear interpolation. We performed two re-optimization passes using this strategy. For each pass, the new solutions were compared against the original 'anomalous' solution and the one with the maximum growth rate was selected (the optimizer cost function maximizes growth rates). This allows us to reduce the impact of local minimum and ensure the results presented were indeed the optimal (global) solution.

Model comparison against proteomic data

We compared the proteomic shifts predicted by the model against proteomic data previously published in the literature for diatom and cyanobacteria species grown under controlled growth conditions. We also compared the shifts in response to warming predicted by the model to data from an experimental evolution study (Aranguren-Gassis et al., 2019). This dataset provided robust evidence supporting the trade-off between investing in transporters versus glycolysis and heat-mitigation strategies (Table S4). The GO terms used for this comparison are given in Table S4. We were unable to find any previous studies that reported the proteomic response of phytoplankton to the multi-stressor growth condition of warming and nutrient limitation. Therefore, we compared the model against other datasets to evaluate the metabolic responses to only nutrient limitation (Table S5). The list of proteins/gene terms used for this comparison is specified below:

Nutrient trasporters: nitrate/ammonia transporters (Remmers et al., 2018), nitrate/ammonium assimilation (Remmers et al., 2018), phosphate-binding protein (Domínguez-Martín et al., 2017), nitrogen assimilation enzymes (nitrate reductase and glutamate synthase) (Yang et al., 2014), nitrate/nitrite transporters (Chen et al., 2018), and phosphate transporters (Chen et al., 2018).

Photosystems: proteins from Domínguez-Martín et al. (2017) are described in their Table 1 and correspond to Cytochrome b559 subunit beta, Photosystem II reaction center protein L, Cytochrome b6-f complex subunit 4, Cytochrome b559 subunit alpha, Divinyl chlorophyll a/b light-harvesting protein PcbE, Divinyl chlorophyll a/b light-harvesting protein PcbD. Others included Fucoxanthin chlorophyll a/c protein (Yang et al., 2014). See also Figure 5B for detailed proteins in Chen et al. (2018) and Figure 5 and Supplementary file I in Remmers et al. (2018).

Rubisco: Ribulose bisphosphate carboxylase and other proteins related to carbon fixation; see Figure 5B for detailed proteins in Chen et al. (2018) and Figure 5 and Supplementary file II in Remmers et al. (2018).

Ribosomes: ribosomal proteins (small and large units); see Figure 5D in Chen et al. (2018).

Glycolysis: KEGG pathways related to Glycolysis/Gluconeogenesis, which includes Embden-Meyerhof pathway (glucose to pyruvate), glycolysis, pyruvate oxidation and gluconeogenesis; see Table S5 in Chen et al. (2018).

Lipid synthesis: KEGG pathways associated with Glycerophospholipid metabolism (see Table S5 in Chen et al. (2018)), and Glycerolipid metabolism, Fatty acid metabolism and elongation (see Supplementary file II in Remmers et al. (2018)).

Supplemental Figures

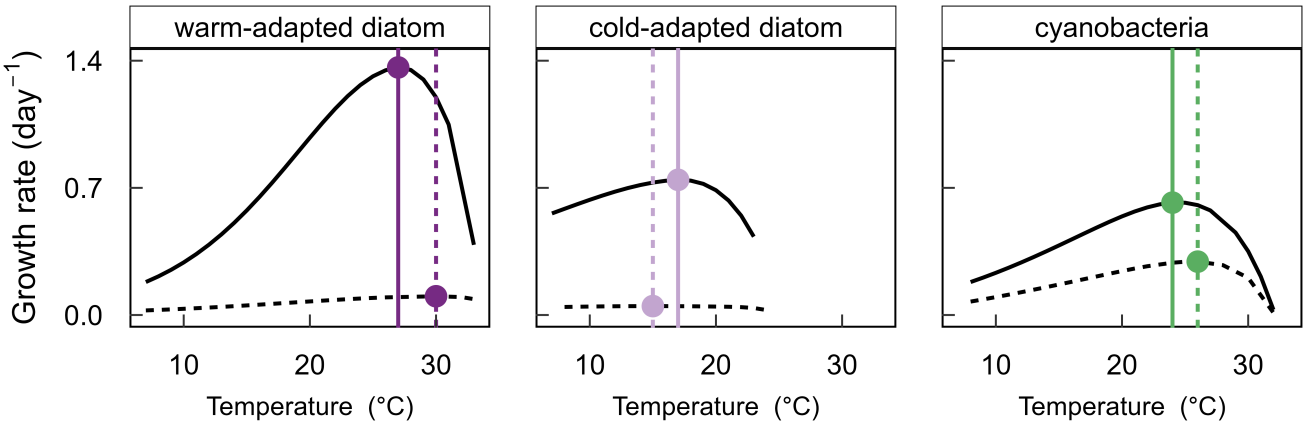

Figure S1: **Emergent thermal growth curves for the different phytoplankton functional types under nitrogen-replete (solid lines; 20 μM) and nitrogen-limiting (dashed lines; 0.01 μM) conditions.** Symbols and vertical lines indicate temperature optima (T_{opt}) in both nutrient regimes. Colors indicate the different phytoplankton functional types following Figs. 3 and 4.

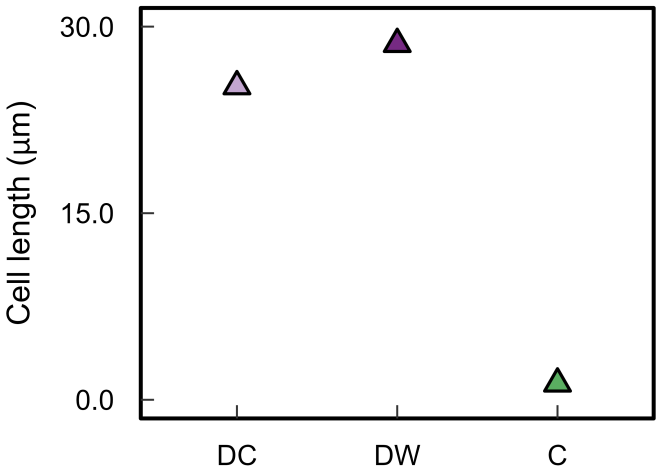

Figure S2: **Cell diameter under nitrogen replete conditions.** Data are given at T_{opt} for each functional type as following: DC: cold-adapted diatom, DW: warm-adapted diatom, C: cyanobacteria. Colors indicate the different phytoplankton functional types following Figs. 3 and 4.

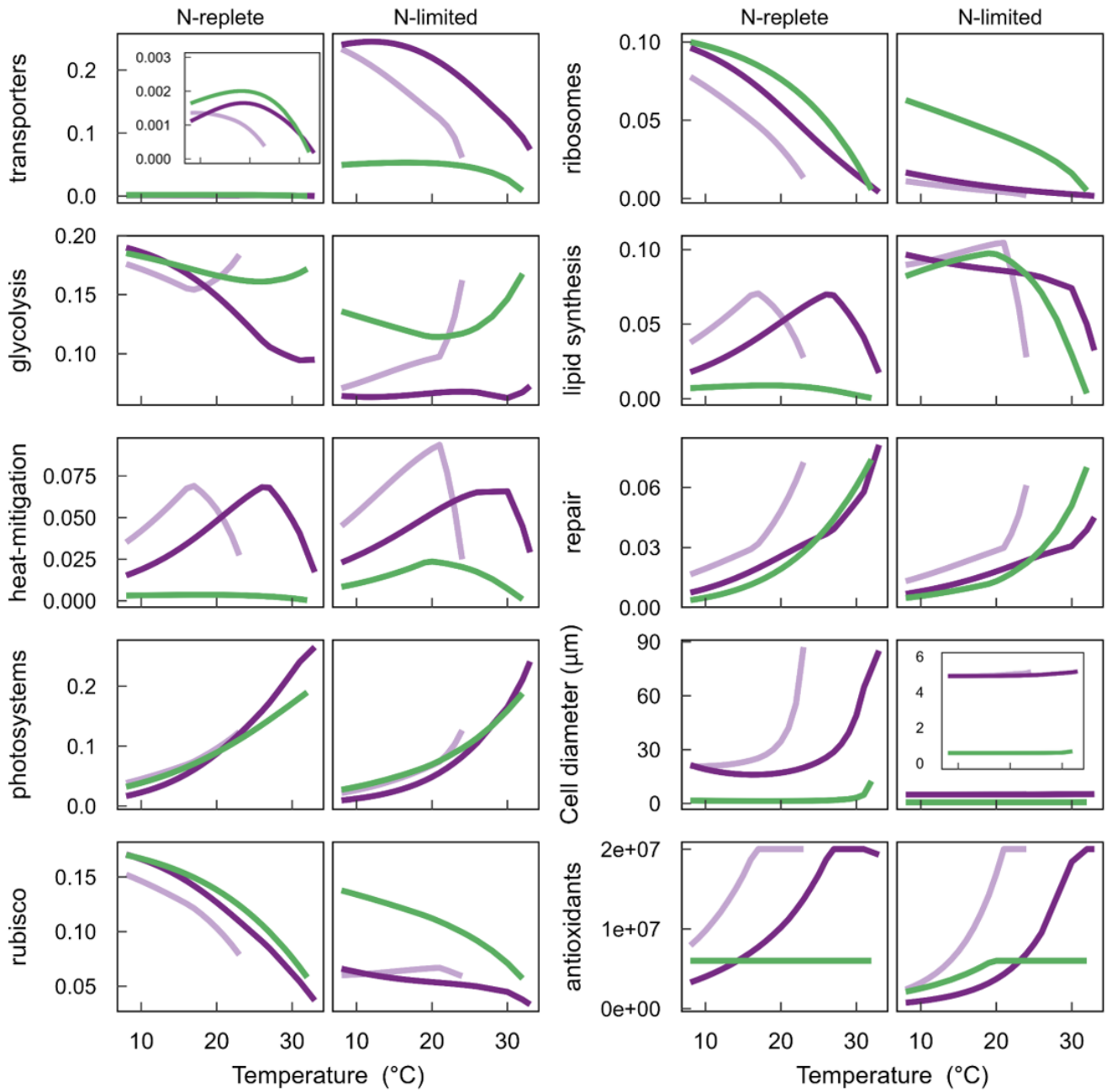

Figure S3: **Optimal relative proteome investments and cell size.** Model output as a function of temperature for N-replete and N-limiting conditions are compared among three phenotypes corresponding to those illustrated in Figs. 3 and 4: (1) cold-adapted diatom (light purple), (2) warm-adapted diatom (dark purple), and (3) cyanobacteria (green). Relative proteome investments vary between 0 and 1 and antioxidants are given in units of number of molecules μm^{-3}.

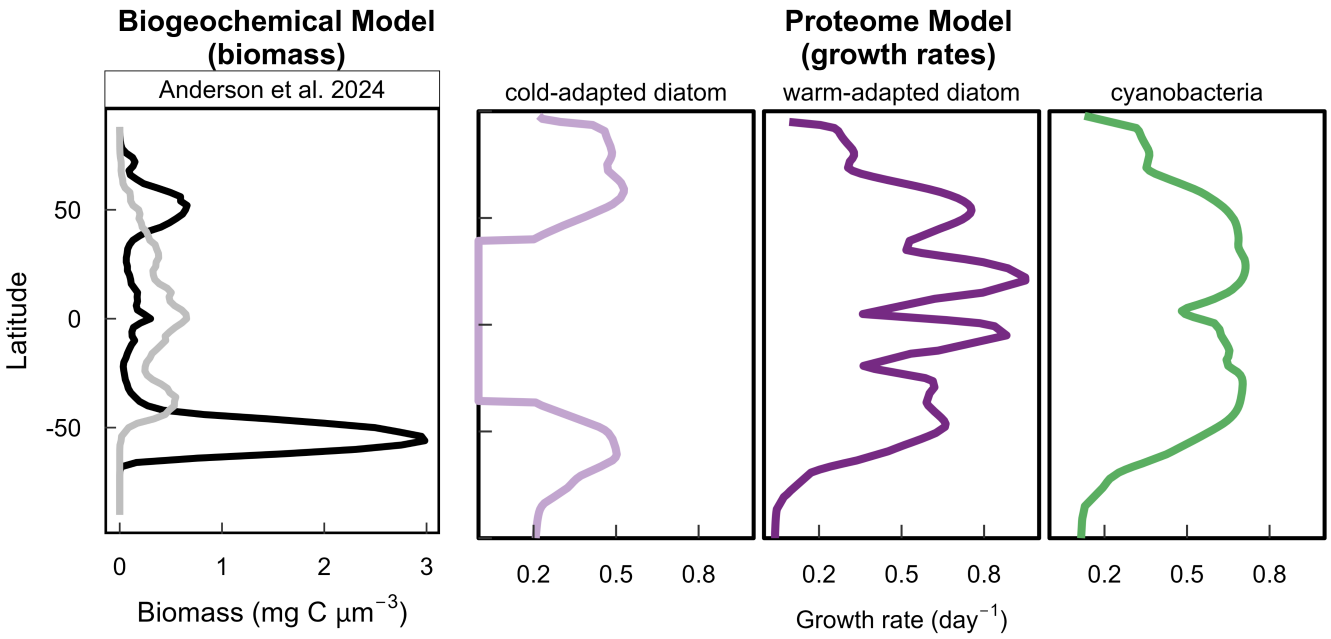

Figure S4: **Mean phytoplankton biomass across a latitudinal gradient from the DARWIN model.** Integrated biomass over the upper 240 m averaged over 10 years is given for diatoms (black line) and cyanobacteria (gray line). Simulated data were obtained from Anderson et al. (2024). Also shown are the optimal growth rates from the proteome model for the different functional types.

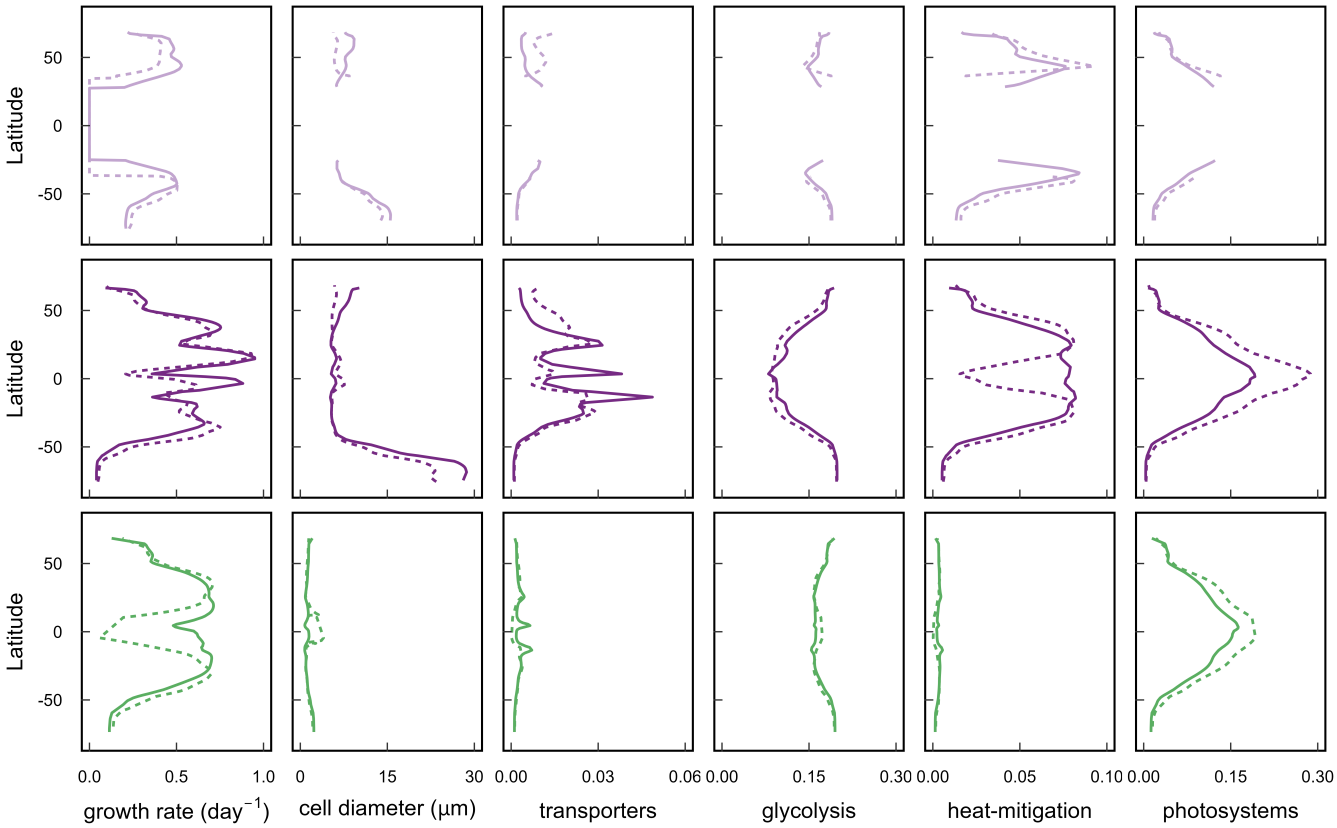

Figure S5: **Phytoplankton optimal metabolic strategies across a latitudinal gradient in the Atlantic Ocean based on temperature and nitrogen concentrations averaged over the upper 20 m of the water column.** Simulations were performed for present-day (1980-2000; solid lines) and future (2080-2100; dashed lines) projections of nitrate concentrations and temperature using model output from the Community Earth System Model (CESM) (Fig. 4A). Results are given for three phytoplankton functional types: cold-adapted diatom (light purple, top row), warm-adapted diatom (dark purple, middle row), and cyanobacteria (green, bottom row). Results are shown for optimal growth rates, cell diameter, and relative proteome investments that vary between 0 and 1. Note that no data is shown for the cold-adapted diatom when growth rates were equal to zero.

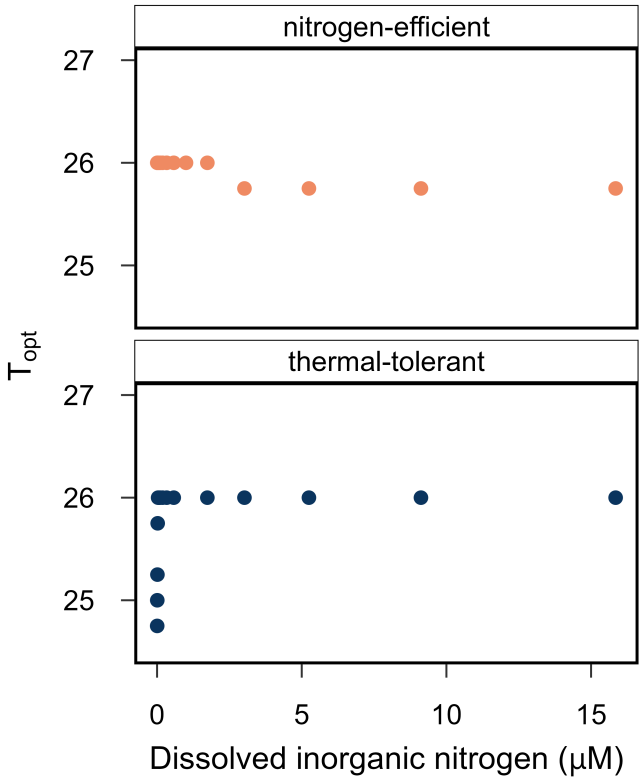

Figure S6: **Temperature optima (T_{opt}) as a function of dissolved inorganic nitrogen (DIN) concentrations.** Simulations are shown for the 'nitrogen-efficient' and the 'thermal-tolerant' strategies. Colors indicate increases in T_{opt} (light pink) or decreases in T_{opt} (dark blue) as a function of decreasing DIN concentrations following Fig. 2C.

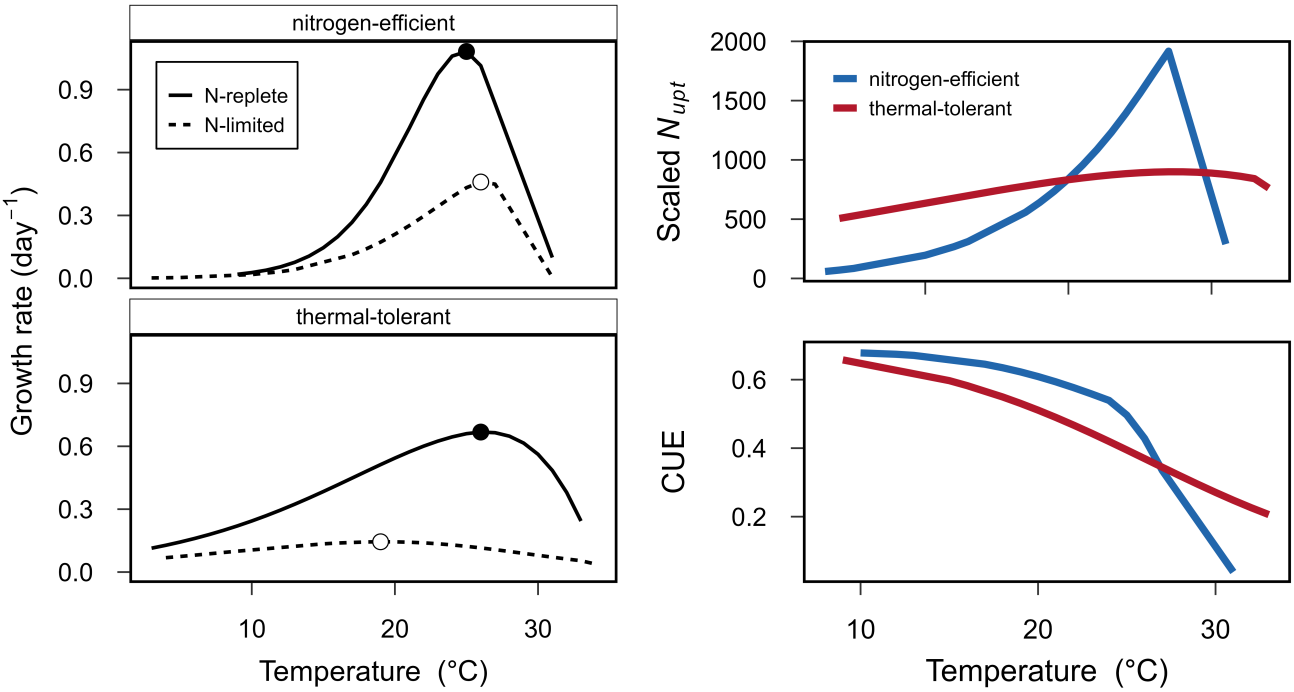

Figure S7: **Model runs where phytoplankton produce antioxidant enzymes to decrease oxidative stress.** (A) thermal growth curves indicate shifts in T_{opt} from nitrogen-replete to nitrogen-limited conditions as a result of different metabolic strategies. (B) model nitrogen uptake rates (N_{upt}) and Carbon Use Efficiencies (CUE) under nitrogen limitation. Carbon use efficiency is defined as 1 - respiration/photosynthesis.

Supplemental Tables

Table S1: **Optimized parameters.** Abbreviations, descriptions and units for the optimized variables. State variables correspond to the concentration of proteins and other macromolecules inside a phytoplankton cell.

	State Variables	
	Proteins	
p_p	Photosystems	molecules of p_p μm^{-3}
p_{ru}	rubisco	molecules of p_{ru} μm^{-3}
p_{tr}	Transporters	molecules of p_{tr} μm^{-3}
p_{ri}	Ribosomes	molecules of p_{ri} μm^{-3}
p_{gl}	Glycolysis	molecules of p_{gl} μm^{-3}
p_{lb}	Lipid Synthesis Pathway	molecules of p_{lb} μm^{-3}
p_{ld}	Lipid Degradation Pathway	molecules of p_{ld} μm^{-3}
p_{re}	Repair Proteins	molecules of p_{re} μm^{-3}
	Other macromolecules	
c_{ic}	Internal Carbon	molecules of C μm^{-3}
c_{in}	Internal Nitrogen	molecules of N μm^{-3}
c_{lm}	Membrane Lipids	molecules of c_{lm} μm^{-3}
p_{ox}	Antioxidants (as lipid storage)	molecules of p_{ox} μm^{-3}
	Parameters	
	Relative proteome investments in proteins	
ϕ_p	Photosystems	unitless
ϕ_{ru}	rubisco	unitless
ϕ_{tr}	Transporters	unitless
ϕ_{ri}	Ribosomes	unitless
ϕ_{gl}	Glycolysis	unitless
ϕ_{lb}	Lipid Synthesis Pathway	unitless
ϕ_{ld}	Lipid Degradation Pathway	unitless
ϕ_{re}	Repair Proteins	unitless
	Other parameters	
β	Volume to Surface Area ratio of the cell	μm
α_{lm}	Fraction of lipid synthesis flux used to build membrane lipids	unitless
α_{ld}	Fraction of lipid synthesis flux used to fuel lipid degradation	unitless
α_{tag}	Fraction of lipid synthesis flux used to build stored lipids	unitless

Table S2: **Parameter values.** Abbreviations, descriptions, values, and units. The values of tunable parameters are given in Table S3. All other parameter values were kept constant across our simulations. See Supplementary Text in Leles and Levine (2023) for references and more details regarding the source of the parameter values.

Maximum reference turnover rates (# molecules per protein per time)			
k_{ref_p}	Photosystems	7800	photons min^{-1}
$k_{ref_{ru}}$	rubisco	157	molecules of C min^{-1}
$k_{ref_{tr}}$	Transporters	120	molecules of N min^{-1}
$k_{ref_{ri}}$	Ribosomes	114	molecules of aa min^{-1}
$k_{ref_{gl}}$	Glycolysis	120	molecules of C min^{-1}
$k_{ref_{lb}}$	Lipid Synthesis	120	molecules of C min^{-1}
$k_{ref_{ld}}$	Lipid Degradation	120	molecules of C min^{-1}
k_{ref_d}	Heat damage	500	molecules of p min^{-1}
$k_{ref_{re}}$	Repair Proteins	1000	molecules of p min^{-1}
Half saturation constants			
K_p	Photosystems	1	μmol photon m^{-2} s^{-1}
K_{ru}	rubisco	1	μM DIC
K_{tr}	Transporters	Table S3	μM DIN
K_{in}	Nitrogen Metabolism	10000	molecules of N μm^{-3}
K_{ic}	Carbon Metabolism	10000	molecules of C μm^{-3}
K_{gl}	Glycolysis	10000	molecules of C μm^{-3}
K_{lb}	Lipid Synthesis	10000	molecules of C μm^{-3}
K_{ld}	Lipid Degradation	10000	molecules of C μm^{-3}
Temperature effects			
E_a	Thermal dependency	Table S3	eV
$E_{a_{tr}}$	E_a of transporters	$E_a/2$	eV
E_d	Deactivation energy	1.4	eV
T_d	Stress temperature	Table S3	$°C$
T_{ref}	Reference temperature	20	$°C$
R	Boltzmann's constant	8.62×10^{-5}	eV/K
Molecular weights			
η_p	Photosystems	9082	aa/molecule of p
η_{ru}	rubisco	5933	aa/molecule of ru
η_{tr}	Transporters	1046	aa/molecule of tr
η_{ri}	Ribosomes	19393	aa/molecule of ri
η_{gl}	Glycolysis	15220	aa/molecule of gl
η_{lb}	Lipid Synthesis	13742	aa/molecule of lb
η_{ld}	Lipid Degradation	5128	aa/molecule of ld
η_{re}	Repair Proteins	6350	aa/molecule of re
η_{in}	Internal Nitrogen	14	Da
η_{ic}	Internal Carbon	12	Da
η_{aa}	Amino Acid	110	Da
η_{gu}	Glucose	180	Da
η_{li}	Lipid Storage	800	Da

Space and density constraints			
s_{tr}	Transporter surface area	1.26×10^{-5}	μm^2
s_{lm}	Lipid surface area	0.5×10^{-6}	μm^2
M_{max}	Transporter to lipid ratio	0.00045	unitless
V_p	Photosystem volume	Table S3	μm^3
V_{li}	Lipid volume	1.5×10^{-9}	μm^3
V_{nu}	Nucleus volume	Table S3	μm^3
D_{max}	Maximum density	1.8×10^{10}	Da μm^{-3}
α	Maximum antioxidant concentration	Table S3	antioxidants μm^{-3}
α_{min}	Minimum antioxidant concentration	200	antioxidants μm^{-3}
Carbon and Nitrogen quotas			
η_{aac}	Amino Acids Carbon	5	C/aa
η_{guc}	Glucose Carbon	6	C/molecule of gu
η_{lic}	Lipids Carbon	16	C/molecule of li
q_{pt}	Protein quota	0.20	N/C
q_p	Photosystems quota	0.10	N/C
q_{ri}	Ribosomes quota	0.33	N/C
Energy conversion factors			
e_p	Photosystems	1.0	ATP/photon
e_{ru}	rubisco	10	ATP/C
e_{tr}	Transporters	1.0	ATP/N
e_{ri}	Protein synthesis	48	ATP/aa
e_{gl}	Glycolysis	5.0	ATP/C
e_{lb}	Lipid Synthesis	3.9	ATP/C
e_{ld}	Lipid Degradation	6.6	ATP/C
e_{re}	Repair Proteins	4.5	ATP/photosystem
e_d	Heat damage	$2.0 \times 10^7/\alpha$	ATP/photosystem

Table S3: **Parameter values for the different phytoplankton functional types.** Parameter values used to parameterize the different phytoplankton functional types represented in our latitudinal simulations, i.e., cyanobacteria, warm-adapted diatom, and cold-adapted diatom. More details and sources can be found in the Supplementary Text.

Parameter	Cyano	Warm-Diatom	Cold-Diatom	Unit	Description
E_a	0.65	1.0	0.65	eV	Thermal dependency
T_d	35	35	25	°C	Stress temperature
K_{tr}	0.05	2.0	2.0	μM	Half-saturation for nitrogen uptake
V_p	1.5e-5	3e-5	3e-5	μm^3	Photosystem volume
V_{nu}	0.1	50	50	μm^3	Nucleus volume
α	6e6	2e7	2e7	antioxidants μm^{-3}	Maximum antioxidant concentration

Table S4: **Comparison between modeled and observed proteomic shifts in response to heat-stress.** Thermal acclimation responses are shown where the arrows correspond to up-regulation (↑) or down-regulation (↓) of pathways from populations growing at temperature optimum to populations subjected to heat-stress. Observations (proteomic data) for the enriched gene ontology (GO) terms correspond to the ancestral populations from an experimental evolution study with the marine diatom *Chaetoceros simplex* growing at 25 °C (optimum) versus the ancestral populations growing at 31 °C (heat-stress) or the warm-evolved populations growing at 34 °C (heat-stress) (Aranguren-Gassis et al., 2024).

Model Variable	Model	GO terms	Ancestral	Evolved
Transporters	↓	nitrate/nitrite transport	↓	↓
		nitrate/nitrite transmembrane transporter activity	↓	↓
		nitrate reductase (NADPH) activity	not enriched	↓
		nitrate assimilation	not enriched	↓
Glycolysis	(↑)	glycolytic process	(↑)	(↑)
		fructose 1,6-bisphosphate metabolic process	(↑)	not enriched
		phosphopyruvate hydratase activity	(↑)	not enriched
		glucose 6-phosphate metabolic process	not enriched	(↑)
Heat-mitigation	(↑)	cell redox homeostasis	(↑)	(↑)
		superoxide dismutase activity	(↑)	not enriched
		removal of superoxide radicals	(↑)	not enriched
		cellular response to oxygen compound	(↑)	not enriched
Repair proteins	(↑)	cellular response to heat	(↑)	(↑)
		cellular response to unfolded protein	(↑)	(↑)
		heat shock protein binding	(↑)	(↑)
		protein folding chaperone	(↑)	(↑)
		misfolded protein binding	(↑)	(↑)
		positive regulation of DNA repair	(↑)	not enriched
		unfolded protein binding	(↑)	(↑)
		protein stabilization	not enriched	(↑)

Table S5: **Comparison between modeled (M) and observed (O) proteomic investment shifts in response to nutrient limitation.** Acclimation responses are shown where the arrows correspond to the up-regulation (↑) or down-regulation (↓) of pathways from nutrient-replete to nutrient- limiting or depleted conditions. Specific protein names used for the comparisons against each modeled pool are given in the Supplementary Methods.

Functional Type	Variable	M	O	Reference
Cyanobacteria	Transporters	(↑)	(↑)	Domínguez-Martín et al. (2017)
	Photosystems	↓	(↑)	Domínguez-Martín et al. (2017)
	Rubisco	↓	↓	Domínguez-Martín et al. (2017)
	Ribosomes	↓	↓	Domínguez-Martín et al. (2017)
	Glycolysis	↓	↓	Domínguez-Martín et al. (2017)
Diatom	Transporters	(↑)	(↑)	Yang et al. (2014); Chen et al. (2018); Remmers et al. (2018)
	Photosystems	↓	↓	Yang et al. (2014); Chen et al. (2018); Remmers et al. (2018)
	Rubisco	↓	↓	Chen et al. (2018); Remmers et al. (2018)
			(↑)	Yang et al. (2014)
	Ribosomes	↓	↓	Chen et al. (2018); Remmers et al. (2018); Yang et al. (2014)
	Glycolysis	↓	↓	Yang et al. (2014); Chen et al. (2018)
			(↑)	Remmers et al. (2018)
	Lipid synthesis	(↑)	(↑)	Yang et al. (2014); Chen et al. (2018)
			↓	Remmers et al. (2018)